IEEE Access
Multidisciplinary | Rapid Review | Open Access Journal

Received November 19, 2018, accepted December 3, 2018, date of publication December 7, 2018,
date of current version January 4, 2019.

Digital Object Identifier 10.1109/ACCESS.2018.2885558

Study on Mutual Coupling Reduction Technique for MIMO Antennas

IRAM NADEEM AND DONG-YOU CHOI, (Member, IEEE)
Communication and Wave Propagation Laboratory, Department of Information and Communication Engineering, Chosun University, Gwangju 61452, South Korea

Corresponding author: Dong-You Choi (dychoi@chosun.ac.kr)

ABSTRACT In recent years, multiple-input-multiple-output (MIMO) antennas with the ability to radiate waves in more than one pattern and polarization play a great role in modern telecommunication systems. This paper provides a theoretical review of different mutual coupling reduction techniques in MIMO antenna systems. The increase in the mutual coupling can affect the antenna characteristics drastically and therefore degrades the performance of the MIMO systems. It is possible to improve the performance partially by calibrating the mutual coupling in the digital domain. However, the simple and effective approach is to use the techniques, such as defected ground structure, parasitic or slot element, complementary split ring resonator, and decoupling networks which can overcome the mutual coupling effects by means of physical implementation. An extensive discussion on the basis of different mutual coupling reduction techniques, their examples, and comparative study is still rare in the literature. Therefore, in this paper, different MIMO antenna design techniques and all of their mutual coupling reduction techniques through various structures and mechanisms are presented with multiple examples and characteristics comparison.

INDEX TERMS Diversity gain, ECC, MIMO, mutual coupling, PCB, UWB, WLAN.

I. INTRODUCTION

Multiple-input-multiple-output (MIMO) [1], [2] is an advanced technology for multiplying the capacity of a radio link using multiple transmit and receive antennas to achieve multipath propagation. MIMO systems specifically refer to a practical technique for sending and receiving multiple independent channels simultaneously over the same radio channel using multiple antenna topologies without any extra radiation power loss in rich scattering environment. It is also featured as next generation wireless communication technology due to its capability of improving system reliability and increasing channel capacity using multiple antennas [3]. MIMO was initially proposed in the early 90's as a feasible solution that can overcome the data rate limitation experienced by single-input-single-output (SISO) systems. Further, MIMO can be used in different networks to improve channel capacity, system reliability and transmission speed of data [4] by utilizing the highest capacity of the wireless communication systems.

In [5]–[10], different printed MIMO antenna systems are presented. These antennas are widely used in the portable systems; such as mobile phones due to their conformity with the device, low cost, better integrity and ease of fabrication. The multi-antenna topology [11], [12] used in the transmitter (TX) and receiver (RX) side in MIMO system makes it simple compared to any other array antenna topology. Further, it improves the data rate in any communication systems [13], [14] by reducing channel errors. However, it leads to multipath propagation problem due to high correlation factor in the multi-signal broadcasting [15], [16]. Moreover, the reduced spacing between the antennas in MIMO can increase the mutual coupling which is a known phenomenon to degrade the angle of arrival [17] to estimate carrier frequency offset [18] and signal to interference noise ratio [19]. The mutual coupling between closely packed antennas rises either by the large flow of surface current from the excited ports or space radiation and surface waves. Additionally, the opposing effect of mutual coupling on reflection coefficients cannot be undervalued [20]. Hence, the major challenge in the design of MIMO antenna is to limit the mutual coupling within the recent miniaturized printed and other antennas. In case of digital infrastructure MIMO systems, the higher mutual coupling has adverse effect on the channel capacity [21] and error rate [22]. A wide range of MIMO precoding and decoding techniques [23], [24]; such as partial swam optimization [25], [26], genetic algorithms [27], [28]

and galaxy based search algorithm [29] are proposed to mitigate mutual coupling in the digital domain. In recent literature surveys, the relationship among MIMO antennas radiation pattern, impedance matrix and beam coupling factors are presented for the mutual coupling of MIMO antenna systems [30]–[32]. Further, comprehensive studies based on these models to mitigate the mutual coupling effects in post processing are also illustrated. However, the simplistic approach for mutual coupling reduction for multi-antenna systems is to use decoupling networks [33], neutralization lines [34], etched parasitic elements [35], complementary split rings resonators [36], electromagnetic bandgap structures [37], and defected ground structures [38]. These techniques can manipulate the coupling by attenuating, blocking or minimizing the surface current flow. The antenna topologies, such as printed, reconfigurable, metamaterials and dielectric resonator antennas are also used popularly to eradicate the adverse effect of the mutual coupling. Furthermore, in MIMO antenna design the envelop correlation coefficient (ECC) evaluation for correlated and uncorrelated channel estimation is necessary [40]. It represents the channel suitability in real propagation systems. There are fewer attempts where mutual coupling reduction techniques are studied and their performances are compared collectively. In [39], a simple comparison on various isolation techniques including decoupling networks, parasitic elements, use of PIN and varactor diode is presented. It also explains the effect on antenna parameters due to different relative permittivity of the substrate materials. A similar study on various miniaturized antenna design for energy harvesting application is presented in [41]. Review on standard mutual coupling degradation techniques for massive MIMO base station antennas are explained in [40]–[42].

In this review paper, a comparative study on different MIMO antenna design methods and mutual coupling reduction techniques is presented. Furthermore, various antenna designs based on every standard mutual coupling technique are analyzed to clarify design variation possibilities. The MIMO antennas presented in this work are discussed and compared with an emphasis on the primary antenna characteristics; such as bandwidth, gain, mutual coupling, efficiency and ECC. Moreover, a brief study on the mutual coupling reduction, diversity gain and envelop correlation coefficient (ECC) calculation methods are described. This work highlights the usefulness and limitations of different MIMO antenna topologies existed in the literature. There are few attempts presented in the literature [12], [39], [40], [42], [44] where the theoretical aspect of the mutual coupling of MIMO antenna is analyzed comprehensively. These works lack to describe different antenna structures corresponding to the MIMO antenna isolation improvement techniques present in the literature. Further, a complete overview containing all the design methodologies and their examples are not present. Therefore, there is a necessity to fill that gap in the field of MIMO antenna design. This review paper offers a thorough analysis on different MIMO antenna and their respective mutual coupling topology to improve the understanding of early stage researchers as well as the experienced antenna designers.

II. MUTUAL COUPLING REDUCTION

Mutual coupling defines as the energy absorbed by a proximate antenna when another antenna is radiating. Mutual coupling has a tendency to change the radiation pattern, reflection coefficient and input impedance of the MIMO antennas. The simplified mutual coupling, MC_{ij} empirical models can be presented as [42], [45]

$$MC_{ij} = \exp\left(-\frac{2d_{ij}}{\lambda}(\alpha + j\pi)\right), \quad i \neq j \tag{1}$$

$$MC_{ij} = 1 - \frac{1}{N}\sum_{i}\sum_{i\neq j} MC_{ij} \tag{2}$$

where $_{dij}$ is the distance between *ith* and *jth* antenna elements. Further, α is the coupling level controlling parameter and N is the number of array elements.

In practice, mutual coupling depends on the array configuration as well as on the excitations of other elements. It is usually calculated in dB-valued S-parameter between *ith* and *jth* antenna elements and the isolation of $-20\log10(|S_{ij}|)$ between them. However, the detailed mechanism of mutual coupling depends largely on the transmitting and receiving modes [46], [47].

In the transmitting mode [42], two antenna elements are in the arrays, as shown in Fig. 1(a). In this case, a source is attached to the *jth* element, A is the energy generated from the source, B points to the energy radiates into space as well as towards the *ith* elements denoted as C. D shows that some part of received energy by *ith* element rescatters into the space while the remaining travels towards the source (E point). A small portion of rescattered energy is picked up by the *jth* element denoted as F. This mutual interaction process continues iteratively. However, after few iterations the rescattered energy D reduces significantly. The total far-field is the vector sum of the rescattered and radiated fields. Therefore, mutual coupling alters the antenna radiation pattern. Moreover, the E waves are added vectorially to the reflected and incident waves of the *ith* element itself causing enhancement in the standing wave. It is responsible to alter the input impedance of the *ith* element. Hence, mutual coupling changes the self-and mutual impedance of the antennas. In MIMO antenna systems, all number of ports may have random phase excitations. This causes significant impact on the impedance matching and mutual coupling of the antenna elements. To evaluate the reflection coefficient of the MIMO systems with random phase excitations total active reflection coefficient (TARC) is calculated [48]. TARC is known as the ratio of the square root of the total reflected power and the total generated power [49]. Higher mutual coupling can reduce TARC due to its dependency on the radiation efficiency and impedance matching under the random phase excitation.

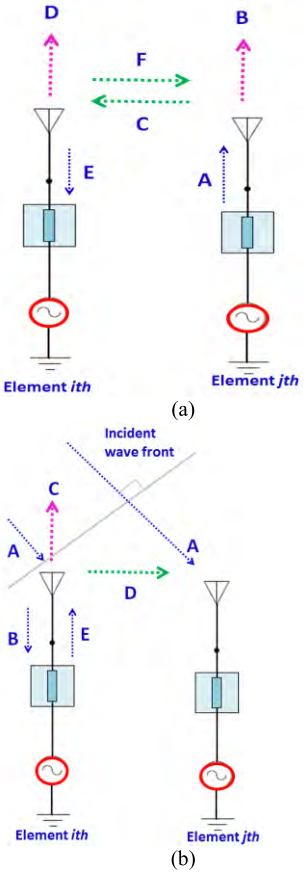

FIGURE 1. Diagram of mutual coupling mechanism (a) Transmitting mode and (b) receiving mode [42].

In the receiving mode, a plane wave A intrudes on the *ith* element causing incident current, as shown in Fig. 1 (b). This incidence plane wave is divided into two parts, one goes. the receiver B w goes into the receiver B while other rescattered into space C. However, some part of the rescattered wave D is directed towards *jth* element. This can be added vectorially with the incident plane wave E. The resultant wave received by the *ith* element is the vector sum of the directed incident wave and the coupled waves from other antenna elements. By minimizing rescattered energy the received energy can be maximized. However, the *ith* element terminating impedance must be chosen carefully as the reflected wave E can cancel the rescattered wave C. Furthermore, the performance of the receiving mode antenna element can be examined by exciting one element with the other 50-ohm loaded element terminal [42].

In case of two-port antenna, the mutual coupling has the tendency to make the antenna pattern orthogonal to each other which effects the correlations. Correlation coefficient describes how much communication channels are correlated or isolated to each other [49]. Signal correlation uses two signals to produce third signal [50]. There are three types of correlations named as power, envelop and signal correlation [47], [51]. Generally, power correlation is equal to the magnitude square of the signal correlation and also

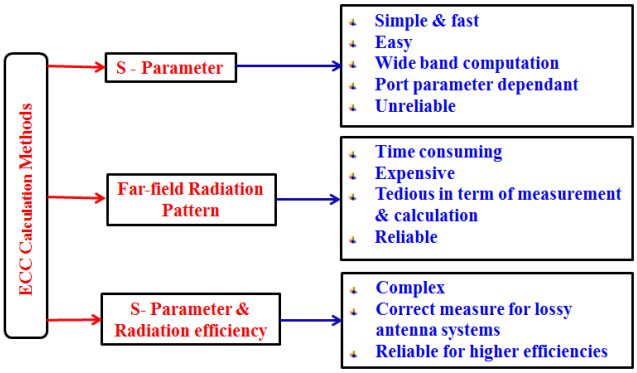

FIGURE 2. ECC calculation methods and performance in MIMO antenna designs.

approximately equivalent to the envelop correlation [47]. The square of the correlation coefficient is also known as the ECC [50]. In this paper, envelop correlation is explained in brief.

III. ECC CALCULATION METHODS AND DIVERSITY GAIN

ECC is the relationship between the incoming signals at the ports of a MIMO or array antenna [52]. In MIMO antennas, ECC is used as a performance metric to characterize and measure the system performance and efficiency. Moreover, ECC evaluation is necessary for uncorrelated channels to find channel quality. Several methods are present in the literature to calculate ECC for MIMO antenna systems [40]. The mutual coupling effect between numbers of ports of MIMO can be observed as two scattering parameters S_{ij} and S_{ji}. High mutual coupling can affect the antenna characteristics adversely. Hence, ECC is increased significantly. Higher value of ECC leads to high correlation and mutual coupling. Therefore, lower ECC values are expected in the MIMO antenna systems [19]. Furthermore, ECC shows combined effect over all the scattering parameters of a designed MIMO antenna to illustrate their effect on correlation coefficients. In typical cellular phone application, ECC value must be less than 0.5 to achieve better diversity [52], [53].

Fig. 2 shows different ECC calculation [8], [54]–[56] techniques along with their performance characteristics. The correlation coefficients for S-parameter calculation method [8], [55] can be approximated as

$$p_{ij}(e) = \frac{\left|\sum_{n=1}^{N} S_{ni}^{*} S_{nj}\right|}{\sqrt{\left(1 - \sum_{n=1}^{N} |S_{ni}|^2\right)\left(1 - \sum_{n=1}^{N} |S_{nj}|^2\right)}} \tag{3}$$

where i $(1 \rightarrow N)$ and j $(1 \rightarrow N)$ are antenna ports, n is the number of radiating elements, S_{ni} and S_{nj} are scattering parameters of antenna elements. This scattering parameters are also knows as reflection coefficients. Network analyzer is used to extract these parameters from the antenna ports of the MIMO system. This approach does not require the

computation and measurement of the radiation pattern of the antenna system. It also offers a clear understanding of the effects of mutual coupling and input Impedance match on the diversity performance of the antenna system.

This is a simple and fast method to calculate ECC which depends on the port parameters of the antenna. However, this technique requires the radiation efficiency to be 100% to perform reliably. It does not consider non-uniform directive patterns. Further, it does not work with beam tilts that affects the channel of upcoming signal and changes system capacity directly [40], [57]. In practice, (3) estimates inaccurate ECC results due to the higher lossy property of the printed antennas. Hence, this methodology of ECC calculation is not prescribed by most of the researchers.

Far-field radiation pattern method uses azimuthal and elevation radiated field components for *ith* and *jth* elements, respectively. Anechoic chamber is used to extract these parameters. The correlation coefficients based on this method [12], [40], [58] is written as

$$p_{ij}(e) = \frac{\left| \iint\limits_{4\pi} \overrightarrow{F_i}(\theta,\phi) \times \overrightarrow{F_j}(\theta,\phi)\, d\Omega \right|^2}{\iint\limits_{4\pi} \left|\overrightarrow{F_i}(\theta,\phi)\right|^2 d\Omega \iint\limits_{4\pi} \left|\overrightarrow{F_j}(\theta,\phi)\right|^2 d\Omega} \tag{4}$$

where $\overrightarrow{F_i}(\theta,\phi)$ and $\overrightarrow{F_j}(\theta,\phi)$ are field pattern of two radiating elements with respect to θ. Additionally, $\emptyset$ and Ω are the solid angles. The evaluation using (4) implies the computation or the measurement of the radiation patterns at each frequency. It must be noted that (3) can be derived from (4) as explained in [40], [8], and [56]. This method is considered as the most accurate and exact for ECC calculation using any number of antenna elements and efficiencies [40]. However, the major drawback in this technique is it requires 3D far field radiation pattern for each antenna elements [59]. Thus, it imposes time constraints as the measurement of far field radiation pattern requires longer period. Additionally, a sophisticated and expensive arrangement is required for this measurement [60].

Third technique is the combination of S-parameter and radiation efficiency [61]–[63]. It offers accurate correlation coefficient calculation by considering the effects of radiation efficiencies of each radiating elements and written as

$$p_{ij.\max} = \frac{-\sum_{n=1}^{N} S_{ni}^{*} S_{nj}}{\sqrt{\left(1-\sum_{n=1}^{N}|S_{ni}|^2\right)\left(1-\sum_{n=1}^{N}|S_{nj}|^2\right)}\,\eta_{rad.i}\eta_{rad.j} + \sqrt{\left(\frac{1}{\eta_{rad.i}}-1\right)\left(\frac{1}{\eta_{rad.j}}-1\right)}} \tag{5}$$

Where $\eta_{rad.i}$ and $\eta_{rad.j}$ are radiation efficiencies of the N-port antenna systems. Compared to other techniques this method requires efficiency calculation as well. However, for the radiation efficiencies below 60 % the value of $\rho_{ij.max}$ is considerably higher. This technique is not suitable for pattern shape or tilted beam [64].

Another method to calculate ECC by far field utilization is given in (6) where $\eta_{\max}$ is the maximum efficiency and it is dependent on the power distribution of the radiating elements. In this method, $\eta_i\eta_j$ is the total efficiency of the radiation elements [65]. It also shows that ECC is dependent on power distribution of radiating elements and efficiency does not depend on radiation efficiencies and S-parameter.

$$\left|p_{ij}(e)\right|^2 = 1 - \frac{\eta_{\max}}{\eta_i\eta_j} \tag{6}$$

There are other methodologies present to calculate correlation coefficients by using antenna equivalent circuits [7], [30], [54], [60]. Some recent literatures [12], [40] explain the method to extract exact value of correlation coefficients from antenna-based series and parallel circuits. Moreover, for fast and accurate ECC prediction of wideband MIMO systems correlation green's function can be used [57]. It works with both frequency domain and time domain post processing techniques. Further, the approximation from S-parameters is based on isotropic assumption in a rich scattering environment. Hence, the best way to calculate ECC is by using far field parameters [40], [44], [66].

Diversity gain (G_{DG}) is another important factor that must be taken into account while evaluating the MIMO performance. It gives an idea about the reliability of the MIMO system [52]. The higher the value of diversity gain the isolation is better [67]. It is dependent on the correlation coefficients between antenna signals is written as

$$G_{DG} = 10 \times \sqrt{1 - \left|\rho_{ij}(e)\right|^2} \tag{7}$$

IV. MIMO ANTENNA DESIGNS AND MUTUAL COUPLING REDUCTION TECHNIQUES

This section describes different MIMO antenna design and mutual coupling reduction techniques [67]. Each technique is explained with multiple recent examples and a comparison table. Fig. 3 lists the MIMO antenna design techniques and mutual coupling reduction techniques focused in this review paper. The performance of every MIMO antenna is compared in terms of isolation level, bandwidth [68], [69], substrate materials, efficiency [70], gain [71], envelop correlation coefficient (ECC) and diversity gain (G_{DG}) [67], [71].

A. DEFECTED GROUND STRUCTURE

Defected ground structure (DGS) represents the defects or slots integrated on the ground plane of planar circuits or antennas [72]. It is adopted as an emerging technique for improving several parameters of microwave MIMO antenna systems including narrow bandwidth, cross-polarization and low gain [73], [74]. Further, this technique contributes significantly to reduce mutual coupling. In this section, recent DGS techniques are described to decrease mutual coupling in the MIMO antennas.

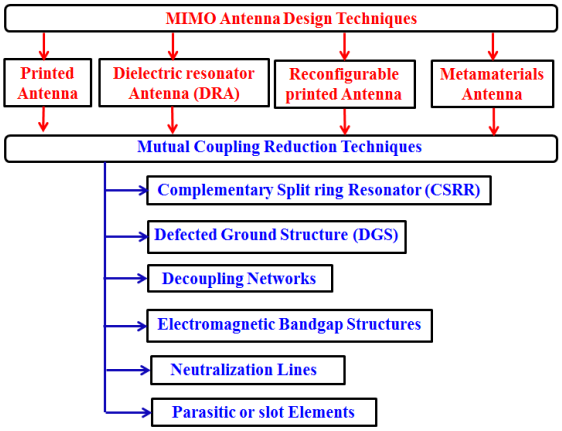

FIGURE 3. MIMO antenna designs and mutual coupling reduction techniques.

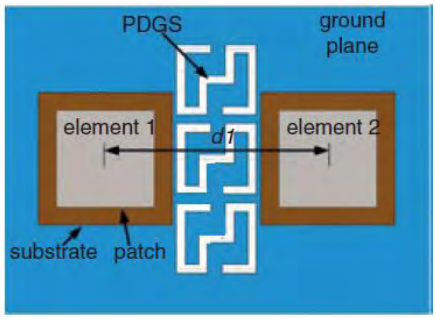

FIGURE 4. PGDS-based MIMO antenna for mutual coupling reduction [75].

1) S-SHAPED DEFECTED GROUND STRUCTURE

In Fig. 4, the periodic S-shaped defected ground structure (PDGS) unit [75], has been placed between antenna radiating elements to reduce mutual coupling. PDGS interrupts the EM far-field significantly and induces the current between patch elements. The coupling between two microstrip antenna elements is the function of relative alignment due to two side by side radiating elements. Without PDGS unit large surface current is induced on the coupled antenna elements results higher mutual coupling. However, in the presence of etched PDGS surface induced current is significantly reduced due to its confinement with in restricted substrate area. Therefore, a higher isolation causes −40 dB lower mutual coupling between the antenna elements.

2) SRDGS DEFECTED GROUND STRUCTURE

Fig. 5 explains the square ring defected ground structure (SRDGS) [76]. This structure has two ports square radiating patch supporting orthogonally polarized half wavelength modes, as shown in Fig. 5(a). Additionally, L-shaped slots are included inside to make this structure compact. Inner patch feed or inside ring ports P1 and P2 excites TM01 and TM10 modes [77]. While two ports P3 and P4 are outside the ring and works on higher order orthogonal modes

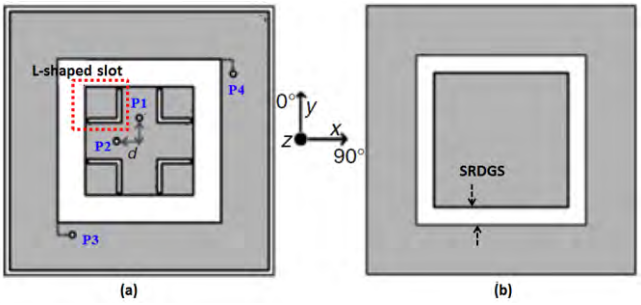

FIGURE 5. SRDGS-based MIMO antenna for mutual coupling reduction. (a) Top layer, (b) Ground layers with DGS [76].

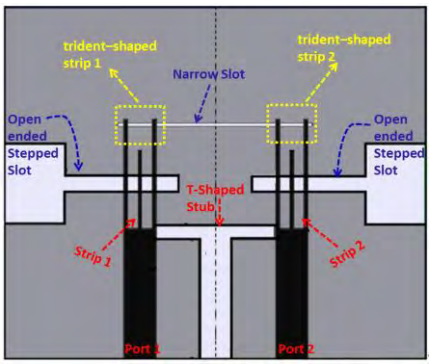

FIGURE 6. T-shaped metallic stub based MIMO antenna for mutual coupling reduction [78].

TM_{21} and TM_{12}. A square ring defected structure is etched in the ground plane, as shown in Fig. 5(b). This acts as a resonant slot to reduce surface waves and decrease cross-polar levels by confining them within dielectric that causes coupling between antenna radiating elements. Further, surface wave reduction leads to less diffraction from corresponding substrate boundary which contributes to back radiation reduction. Consequently, increased isolation is developed between ports.

3) T-SHAPED METALLIC STUB BASED DEFECTED GROUND STRUCTURE

In Fig. 6, two open ended slots are added in the ground plane [78] to implement DGS feature. It improves isolation between antenna elements in the ultra-wide band (UWB) range. Further, it provides band-notch functionality from 5.4 ∼ 5.86 GHz and 7.6 ∼ 8.4 GHz due to the presence of trident–shaped strip on microstrip feed line. Moreover, ground plane consists of a middle T-shaped metallic stub. Two open-ended stepped slots etched in parallel with very narrow slot. This T-shaped slot suppresses the surface current and diverts its direction. Therefore, it increases the distance between the ports to improve isolation in between the antenna elements. It is also referred as decoupling slot. The purpose of the narrow slot is to provide better isolation at lower resonant frequency of 3 to 4 GHz. This can reduce the mutual coupling up to −20 dB. On the other hand, the open-ended

TABLE 1. Performance comparison of DGS MIMO antennas.

Ref.	Dimensions (mm^3) / Material	Isolation Level(dB)	Technique Employed	Gain / Radiation efficiency	ECC/DG	Application / No. of ports	Remarks
[75]	100×72×3.81/ **RogersTMM6**	≥ -55dB at 2.57 GHz	S-shaped periodic DGS	-1.79 ~ 3.75dBi/ 93 ~ 96%	NG/NG	WLAN/ Quad ports	Large thickness and high efficiency
[76]	60.2×60.2×1.6/ **FR-4**	≥ -25dB at 2.45GHz	Square ring DGS	2.1dBi/ 81%	≤ 0.1(S-parameters)/ 9.94 dB	WLAN/ Quad ports	Compact structure and easy fabrication
[78]	22×26×0.8/ **FR-4**	≥ -20dB at 3.1 ~ 11.8 GHz	Ground plane open ended slot and trident–shaped strip	3.6~6 dBi /85%	≤ 0.03(S-parameters)/ 9.99 dB	UWB, WLAN , X- band notched / Dual ports	Compact structure and high bandwidth and filter
[38]	50×160×0.8/ **FR-4**	≥ -20dB 0.7 ~ 1.0 GHz	Open ended DGS-slots	2 dBi/ 80%	≤ 0.075 (Far-Field Radiation pattern)/ 9.97 dB	LTE / Quad port	Complex structure and control-able mutual coupling

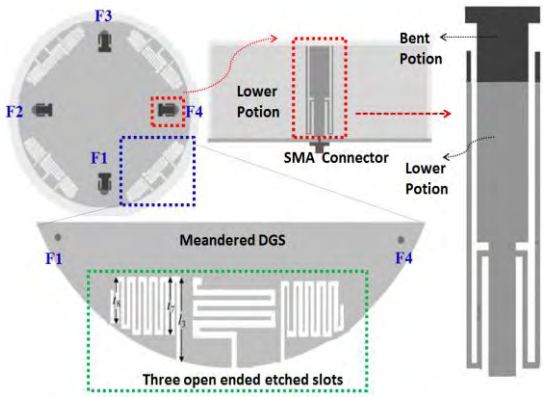

FIGURE 7. Electrically small meandered based MIMO antenna for mutual coupling reduction [38].

slot on ground plane provides better impedance matching characteristics in lower frequency bands. The trident–shaped strip is a combination of rectangular slot and loaded strip fed by microstrip line, is implemented on top of the substrate. In Fig. 6, theses strips are illustrated as strip-1 and strip-2. These are responsible to generate dual notches at 5.7 and 8.2 GHz.

4) ELECTRICALLY SMALL MEANDERED DEFECTED GROUND STRUCTURE

Fig. 7 shows top-loading monopole antenna [38] with a sleeve attached on each side of the radiating body utilizing multi-object optimization technique. It consists of cylindrical shape with four evenly spaced antenna elements around its circumference with reference to the center of the circle. At lower and higher frequencies the surface current concentrated on radiating portion of the monopole and sleeves, respectively. The DGS technique is utilized by using three open ended etched areas on the metallic ground plane. This architecture acts as a band stop filter to reduce the amount of induced currents. These three slots are used to achieve required frequency 0.8 GHz and reduce mutual coupling upto −25 dB. Further, there is a bent in the outer slots of DGS to utilize minimum spacing in the ground plane. An open-ended slot is also implemented by using quarter wavelength calculation to act as a bandstop filter [79]. Furthermore, these slots are symmetrically constructed to minimize the opposing effects of DGS on radiation pattern [80]. The spacing between the slots of DGS is the main feature of this antenna. It can adversely affect the impedance matching and mutual coupling. Therefore, spacing of 0.24 λ between two slot elements is considered for optimal performance.

Characteristics of different DGS antennas described in this section are summarized in Table 1. It shows that the antenna in [75] has highest dimensions and thickness. It achieves maximum efficiency and minimum mutual coupling of −55 dB compared to other antennas presented in Table 1. Further, [78] provides maximum bandwidth along with band notch feature and compact dimension. However, it shows significantly lower mutual coupling performance compared to [75].

B. DIELECTRIC RESONATOR ANTENNA

Dielectric resonator antenna (DRA) [81], [82] uses various shapes of ceramic material blocks fixed on metal surface or ground plane. DRA is used to transform guided waves into unguided RF signals [83] for transition through vacuum, air or water. In this section, cylindrical dielectric resonator antennas (CDRAs) are considered which is one of the primary types of DRAs. This antenna exhibits higher efficiency and lower loss compared to complete metal antennas due to minimum metal part for millimeter wave frequencies [84], [85].

1) BACK-TO-BACK CDRA-BASED MIMO ANTENNA

Fig. 8 shows back-to-back element CDRA-based antenna placed on the opposite sides of the substrate through common

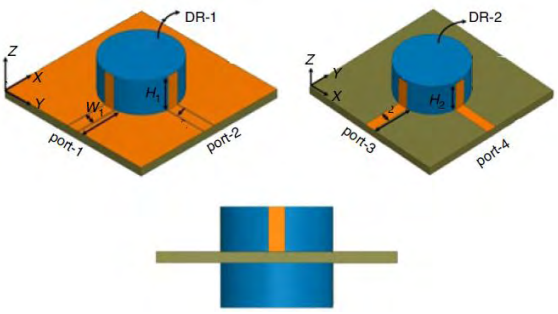

FIGURE 8. CDRA-based MIMO antenna to reduce mutual coupling [86].

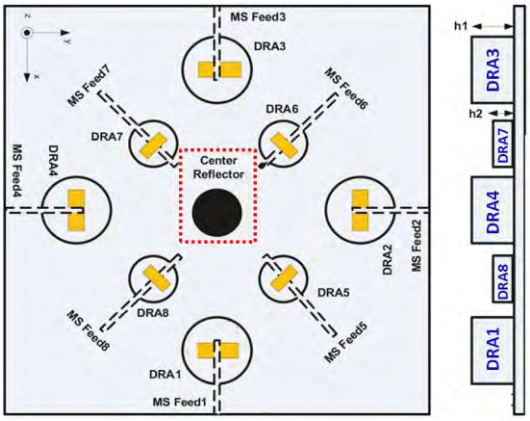

FIGURE 9. Eight ports DRA based MIMO antenna with center reflector for mutual coupling reduction [87].

ground plane [86]. A pair of co-planar waveguide (CPW) conformal microstrip lines is used to excite port-1 and port-2. The height of the top and bottom CDRAs are 6.5 mm and 6.0 mm, respectively. Port-3 and port-4 are excited by microstrip line fed conformal strip line. Improved isolation level between all ports is achieved by generating orthogonal modes $HE^{y}_{11\delta}$ and $HE^{x}_{11\delta}$ in each CDRAs. Further, the use of opposite excitation also contributes to the isolation improvement. In this case, both the CDRAs are excited in opposite directions which produce bidirectional pattern diversity. In this geometry, $HE_{11\delta}$ mode radiates in broadside direction. Two ports in a single CDRA generate two orthogonal patterns due to the difference in the polarization. In summary, using orthogonal modes and the excitation from opposite directions contribute to the improvement on the isolation between the ports significantly.

2) DUAL SHAPE CDRA AND METALLIC REFLECTOR BASED MIMO ANTENNA DESIGN

Fig. 9 demonstrates eight port dual band CDRA MIMO antenna system [87]. The geometry involves four antennas (labeled DRA1 to 4) of 55 mm radius placed at 90° angles along the center reflector circle. Further, other four antennas (labeled DRA5 to 8) of 30 mm radius are placed near the center reflector circle and are in 45° angles with DRA1 to 4. The optimized DRA height is 14 mm and 5mm for better

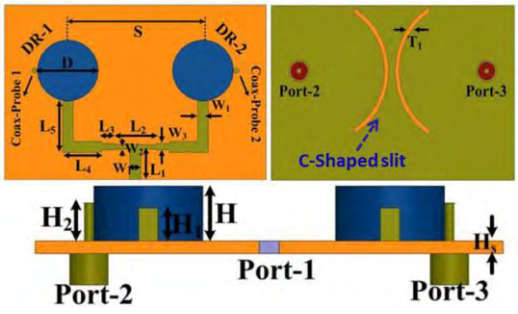

FIGURE 10. Hybrid based technique (dual mode CDRA, power divider based matching network and slit) for MIMO antenna design and improving isolation [88].

isolation. Antenna elements are excited by slot coupling mechanism through microstrip transmission line which is mounted at the bottom of the substrate. These coupled slots are exactly beneath the CDRA. DRA 1 to 4 produce modes of $HEM_{11\delta}$ kind while $TE_{01\delta}$ modes excitation is visualized at DRA 5 to 8. The better coupling between coupling slot and CDRA is achieved by using different dimension feed lines for higher (5.8 GHz) and lower bands (2.45 GHz).

However, center reflector of 30 mm and height 40mm are used to achieve maximum isolation of −25dB.

3) C-SHAPED SLIT AND DRA FOR MIMO ANTENNA DESIGN

Fig. 10 explains a hybrid technique with triple port dual mode CDRA-based MIMO antenna systems [88]. Port 1 consists of two λ/4 impedance transformers which is known as power divider to match the feeding network. CDRAs at port 2 and port 3 are excited by the coaxial probe which helps in generation of orthogonal modes known as $HE^{y}_{11\delta}$ and $HE^{x}_{11\delta}$. Ground plane containing etched C-shaped slit (DGS technique) is used to improve isolation and lower mutual coupling to −25 dB by maximizing the surface current distribution at the excited ports and around the C-shaped slit.

4) ANNULAR METALLIC RING BASED DRA ANTENNA FOR HIGHER ISOLATION

In Fig. 11, a hybrid MIMO antenna is presented with CDRA and modified printed annular ring shape [89]. These modified rings are responsible for the generation of two different radiating modes $HE_{11\delta}$ and $TE_{01\delta}$. For the reduction of mutual coupling and improving isolation at lower frequency (1.75 ∼ 2.4 GHz) a narrow rectangular slit (DGS technique) in the ground plane is etched. This slit blocks the surface current distribution from excitation port 1 to port 2.

Further, CDRA is orthogonally placed over the annual ring to improve isolation in upper frequency of 3.5 ∼ 5.5 GHz. Therefore, a non-overlapping E-field is generated due to radiating modes.

The characteristics of the DRA antennas explained in this section are summarized in Table 2. It shows that the antenna presented in [89] has highest isolation achieved at −25dB with a dual band property. Further, [87] demonstrates highest gain and efficiency.

TABLE 2. Performance comparison of DRA MIMO antenna.

Ref.	Dimensions (mm^3) / Material	Isolation Level(dB)	Technique Employed	Gain / Radiation efficiency	ECC/DG	Application / No. of ports	Remarks
[86]	30×30×13.6/ **FR-4 (1.6 height)**	≥ -18dB at 5.4 ~ 6.0 GHz	Alumina ceramic DRA material , ε_r = 9.8 and back to back placement ,	5dBi / NG	> 0.25 (Far-Field Radiation pattern)/ 9.8 dB	WLAN/ Quad ports	Compact structure and bidirectional pattern diversity
[87]	160×160×14.8/ **RO3003 (0.762 height)**	≥ -15dB at 2.45 GHz and 5.8 GHz	HiK500 DRA material , ε_r = 10 , Metallic reflector, Glue (ε_r = 3.3 , thickness ~ 100 µm)	2.45GHz = 6.5dBi / 97% 5.8GHz = 8.9dBi / 98%	≤ 0.037(S-parameters)/ 9.99 dB	WLAN / Eight ports	Complex geometry and higher No. of ports. max. gain and efficiency.
[88]	40×60× 8.6/ **FR-4 (1.6 height)**	≥ -20dB at 5.15 ~ 6.0 GHz	Alumina ceramic DRA material , ε_r = 9.8 , C-shaped slit	5 dBi / 88%	≤ 0.2 (Far-Field Radiation pattern)/ 9.79 dB	WLAN / triple ports	Hybrid technique due to power divider matching structure
[89]	60×60× 8.6/ **FR-4 (1.6 height)**	≥ -25 dB at 1.75~2.4 GHz and ≥ -20 dB at 3.5~5.5 GHz	Metallic modified annular ring , Alumina ceramic DRA material , ε_r = 9.8	3 dBi / 82% ~ 90%	≤ 0.05 ~ 0.16 (S-parameters) / 9.94 ~ 9.05 dB , CCL = 0.5 bits/s/Hz	GSM , 3G, WLAN / Dual ports	Simple structure and dual band operation

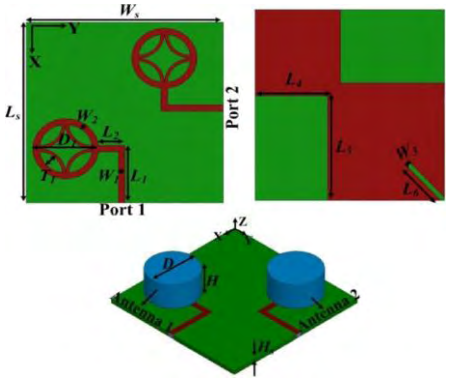

FIGURE 11. Annular ring DRA MIMO antenna for mutual coupling reduction [89].

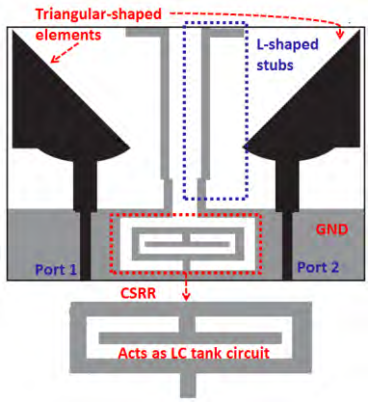

FIGURE 12. Ground loaded CSRR based MIMO antenna [36].

C. COMPLEMENTARY SPLIT RING RESONATOR

Complementary Split ring Resonator (CSRRs) are usually periodic configurations [90], [91] of metallic ring, shunt strip or capacitive gap used to perform filtering as well as isolation improvements function and lower mutual coupling.

1) GROUND PLANE CSRR BASED MUTUAL COUPLING REDUCTION

Fig. 12 shows triangular-shaped radiating elements [36] to achieve wideband impedance matching as the monopoles cannot radiate towards each other directly. This allows space reduction between radiating elements. However, it fails to exhibit higher isolation at entire UWB. To improve the isolation and make mutual coupling less than −15 dB two segmented L-shaped stubs are inserted in the ground plane. These stubs have length of $\lambda_o/4$ (λ_o at 3.8 GHz). These stubs serve as reflector to reduce mutual coupling between monopole radiating elements by separating radiation between them [92]. Further, it introduces two resonances (at 3.8 GHz and 6.8 GHz). To reduce mutual coupling significantly at lower frequency CSRR has been added in the ground plane. Hence, this technique also reduces the size of the antenna. Additionally, this CSRR acts as an LC tank circuit which can store the energy at lower frequency and blocks the current in the ground to reach other antenna elements. Therefore, CSRR is used to prevent the current flow between antenna elements to improve the antenna isolation.

2) CONCENTRIC SQUARE RING PATCH WITH CSRR LOADED GROUND PLANE

In Fig. 13, quad port MIMO antenna containing concentric square ring radiating patch [93] is presented to resonate in

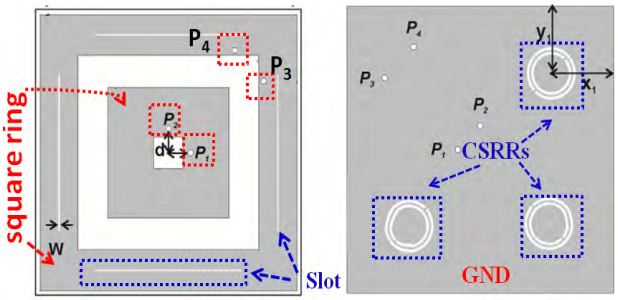

FIGURE 13. Concentrate square ring and CSRR loaded MIMO antenna [93].

different transverse magnetic modes. Further, three resonant structure of CSRRs are etched in the ground plane. These CSRRs have sub-wavelength value at resonant frequency of 2.45 GHz. The purpose of concentric square ring is to enhance the bandwidth due to lower amount of energy stored in the metallic regions. The second square encloses the inner ring and makes the structure compact is size. The feed position is selected in a way to excite higher order modes orthogonally by maintaining higher isolation between them. Further, for higher modes with non-zero substrate thickness the surface wave propagation is also high. Thus, reactive loading in antenna is adopted by etching a slot on each square ring to improve this performance. The slots have length of $\lambda/2$ at resonant frequency of 2.45 GHz. This slot is also the source of mutual coupling reduction between higher order modes generated in rings. Three CSRRs are etched in the ground plane around the corners of the antenna tilted at 45° angle. The presence of CSRRs alters the standing wave distribution by generating higher coupling current. This reveals the resonant property in vertically polarized fields as well. Therefore, the two ports P_1 and P_4 of the antenna work on the vertically polarized electromagnetic (EM) wave and other two ports P_2 and P_3 deal with horizontal polarized EM waves. This configuration ensures least mutual coupling between them resulting good isolation.

3) TRADITIONAL PATCH ANTENNA WITH CSRR LOADED GROUND PLANE

Fig. 14 explains another type of quad port MIMO antenna [94] containing traditional patch antenna in the upper plane of substrate while four CSRRs in the bottom plane.

These CSRRs modeled as LC circuit control the resonant frequency by interacting with the electric field. Additional half space in the ground plane is also used to support different electronic devices within the standard PCB board size. In this work, the CSRRs consist of a pair of slit rings which are oriented in such a way that the open parts are towards the port of the radiating patch element. Furthermore, the opening of outer ring slit is positioned towards the edge which is excited by microstrip feed. Moreover, the inner slit ring is printed in the opposite direction of the radiating patch feed line.

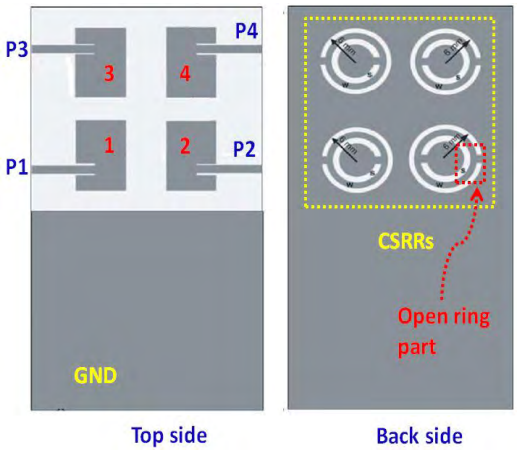

FIGURE 14. Ground plane center etched CSRR between feed ports for low mutual coupling [94].

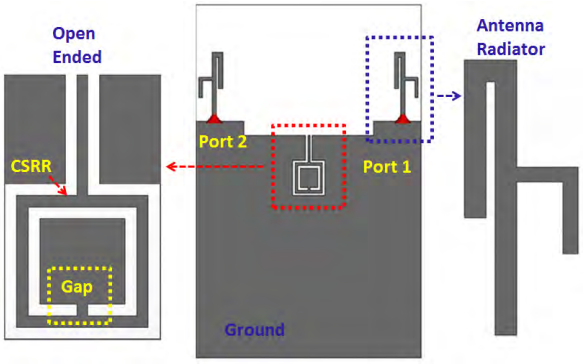

FIGURE 15. Ground plane center etched CSRR between feed ports for low mutual coupling [95].

4) SLOTTED CSRR IN GROUND PLANE

Fig. 15 shows a CSRR where two identical (homogenous) antennas are used as radiating elements separated from each other to improve isolation by etching a CSRR in the ground plane [95]. It is also known as space diversity utilization technique. In this design, only one CSRR is used to improve isolation, hence by adjusting the length of CSRRs slit isolation can be easily adjusted. The distributed capacitance of the slotted CSRR is increased with the increase in the gap between slit's lengths. This CSRR also has the ability to miniaturize the antenna as it has open end.

Table 3 lists the characteristics of CSRR antennas presented in this section. In [95], higher efficiency of 86.62 % and simplest geometry with dual band characteristics is achieved. It also demonstrates lowest ECC value. Further, it has better isolation and lower mutual coupling of −33 dB. Therefore, [95] can be considered as the better structure compare to other CSRRs presented in this section.

D. NEUTRALIZATION LINES

Neutralization lines [96], [97] are used to pass the EM waves from one antenna to the other through metallic slit or

TABLE 3. Performance comparison of CSRR MIMO antennas.

Ref.	Dimensions (mm^3) / Material	Isolation Level(dB)	Technique Employed	Gain / Radiation efficiency	ECC/DG	Application / No. of ports	Remarks
[36]	23×29×1.524/ **Rogers TMM4**	≥ -15dB at 3 ~ 12 GHz	Ground CSRR and stub	5.9dBi / 82%	≤ 0.15(Far-field radiation pattern)/ 9.88 dB	UWB / Dual port	Compact structure and high bandwidth
[93]	60×60×1.6/ **FR-4**	≥ -22dB at 2.2 ~ 2.7 GHz	Concentric square ring patch and ground CSRR	4dBi / 72.5%	= 0.4(Far-field radiation pattern)/ 9.16 dB	ISM/Quad port	Simple geometry , vertical and horizontal polarized
[94]	100×50×0.8/ **FR-4**	≥ -18dB at 2.4 ~ 2.5 GHz	Bottom plane CSRR and ground plane	-0.8 dBi / 29%	≤ 0.3(S-parameters)/ 9.53 dB	ISM/Quad port	Lower thickness and large dimensions
[95]	70×100×1.6/ **Rogers4003**	≥ -20dB at 2.45GHz and ≥ -33dB at 5 GHz	Slotted CSRR in ground plane	4.025 dBi / 86.64 %	≤ 0.016 (S-prameters and Far-Field)/ 9.99 dB	WLAN/Dual port	Simple geometry, max. Isolation and dual band

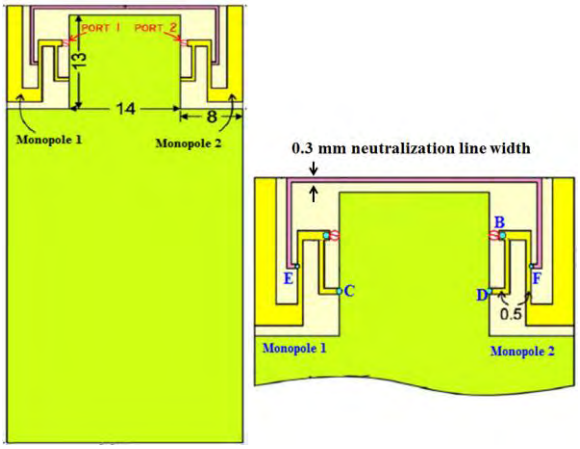

FIGURE 16. Thin neutralization lines between symmetric monopoles for mutual coupling reduction [98].

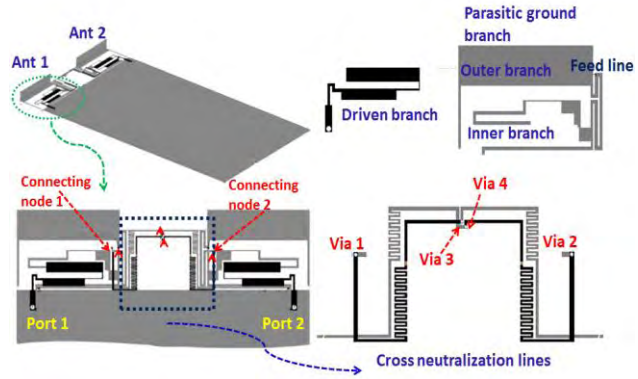

FIGURE 17. A driven branch and two crossed neutralization lines for low mutual couplings [99].

lumped element. Hence, an opposite coupling is created to lower the mutual coupling at certain frequencies between the antennas.

1) THIN PRINTED NEUTRALIZATION LINES

Fig. 16 describes a printed MIMO antenna containing two simple short-circuited monopoles [98] located at opposite corners of the substrate and spaced apart by small ground portion. This small ground also acts as a layout area for antenna feeding networks. A thin printed neutralization line is etched close to the antenna feeding to link the monopoles. The purpose of the neutralization line is to enhance the isolation. However, there is no slit cut in the ground plane and it is reserved for coaxial line feeding network or I-PEX connectors. Both the monopole radiating elements are $\lambda/4$ apart at the resonance frequency. Point C and D indicate the short circuiting strips and their length and width variation can be used to control impedance matching. The neutralization line is a simple conduction line of smaller width to reduce the antenna area. By varying the neutralization line length, location and connecting points E and F the isolation properties can be controlled. Further, it can also affect the impedance bandwidth.

2) PAIR OF CROSSED NEUTRALIZATION LINES

Fig. 17 shows a dual band MIMO antenna containing two symmetric antenna elements and two crossed neutralization lines [99]. The antenna elements include a parasitic ground plane and a driven branch. The parasitic ground plane is also a branch network containing inner branch and outer one printed on the bottom layer. Further, the driven branch is on the top layer of PCB. The major portion of the outer branch of the parasitic branch is folded for space diversity and two extended copper sheets are positioned on PCB's upper two corners. The cross neutralization lines are constructed using four vias. Thus, each neutralization line finds connection through vias to non-corresponding antenna element nodes at both ends. The parasitic ground plane and driven branch at antenna terminal generates multi-resonance modes. However, to mitigate the effect of mutual coupling at lower frequency crossed neutralization lines between both antennas elements are included. Furthermore, to reduce mutual coupling at higher frequency of 2.45 GHz the parasitic ground branch

TABLE 4. Performance comparison of neutralization lines MIMO antennas.

Ref.	Dimensions (mm^3) / Material	Isolation Level(dB)	Technique Employed	Gain / Radiation efficiency	ECC/DG	Application / No. of ports	Remarks
[98]	30×65×1/ **FR-4**	≥ -15dB at 2.4 ~ 2.5 GHz	Neutralization line	2.1dBi / 81%	≤ 0.006 (S-parameters)/ 9.8 dB	WLAN USB-Dongle / Dual port	Compact structure and simple geometry
[99]	135×80×0.8/ **FR-4**	≥ -23dB at 750 MHz , 850 MHz , 2.0 GHz and 2.5 GHz	Crossed neutralization line with embedded inductors	-1.79 ~ 3.75 dBi / 31.86 ~ 61.73%	0.180 ~ 0.081(S-parameters)/ 9.8 ~ 9.97 dB	LTE, GSM, WLAN/ Dual ports	Complex structure and max. mutual coupling
[34]	50×40×1.6/ **FR-4**	≥ -20dB at 2.45GHz and , 5.8 GHz	Neutralization line with pair of inductor and capacitor	NG / 78 ~ 85%	0.002 ~ 0.006 (S-parameters) /9.99 ~ 9.999 dB	WLAN/ Dual ports	Simple geometry and high efficiency
[100]	4*×4*×1.6/ **FR-4** *=cm(centimetre)	≥ -21dB at 3.1 ~ 11 GHz	Stepped neutralization line	3.28 ~ 4 dBi / NG	≤ 0.004(S-parameters)/ 9.99 dB	UWB / Quad ports	Large size, simple structure and max. bandwidth

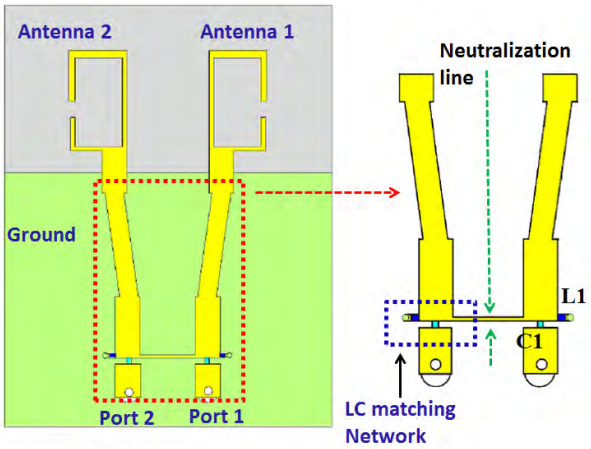

FIGURE 18. LC matching network and neutralization line based MIMO antenna [34].

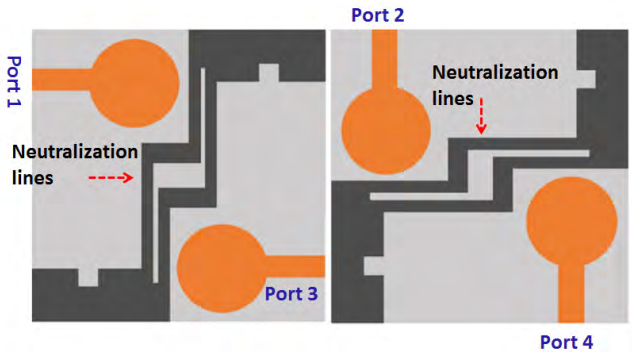

FIGURE 19. Ground plane neutralization lines for mutual coupling reduction [100].

is designed. Hence, crossed neutralization and parasitic ground branch helps to compensate mutual coupling along with a driven branch and vias.

3) LC MATCHING NETWORK AND NEUTRALIZATION LINE

In Fig. 18, a novel antenna is proposed by implementing the neutralization lines in between two coupled dual band antennas [34]. C-shaped radiator is adopted to make the antenna design compact in size. This design principal involves two closely spaced antennas with phased shifting elements. Further, admittance matrix transformation is used for lossless network. For perfect impedance matching the lossless admittance matrix must be purely imaginary number and mutual admittance is a complex number. For better isolation of the ports the off diagonal elements of admittance matrix should be zero. Stepped impedance transformer with two sections is used as a phase shifting network to make mutual admittance a pure imaginary number. Further, a neutralization line is inserted in parallel with the C-shaped radiator antenna as phase shifting elements. This straight neutralization line can produce opposite coupling to generate admittance imaginary number. A LC matching network is added on each port of the antenna to provide better isolation. Therefore, the neutralization line cancels out the unwanted coupling at second port when port 1 is excited.

4) NEUTRALIZATION LINES BETWEEN GROUND PLANES

Fig. 19 demonstrates a planner antenna utilizing neutral slots [100] between ground planes. This four port antenna consists of circular monopole radiating elements feed by microstrip line. Two ports are mounted on the upper side of the substrate and two at the lower side. All four radiating elements are orthogonal to each other. Partial ground plane with very small rectangular slot is introduced to improve bandwidth. Further, microstrip multimode resonator (MMS) principal is adopted by connecting partial ground plane to increase isolation between antenna elements. In this work, neutralization lines act as a band stop filter to minimize surface currents.

Table 4 explains the neutralization-based MIMO antenna characteristics illustrated in section IV.D. In [99], a pair of crossed neutralization line is presented with minimum substrate thickness and acceptable gain values. However, the geometry of the antenna is complex compared to other antennas presented in this section. It works on multiple

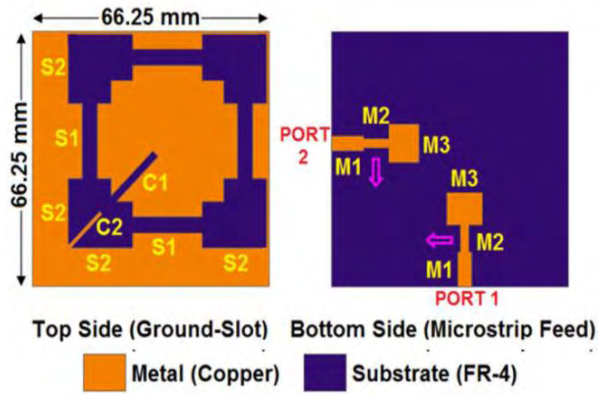

FIGURE 20. Ground plane neutralization lines for mutual coupling reduction [105].

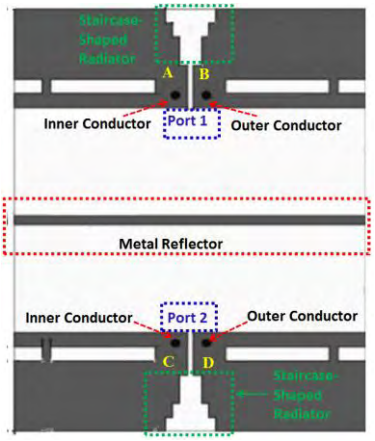

FIGURE 21. Staircase-shaped radiator and middle reflector for mutual coupling reduction [107].

frequency bands and provides the maximum isolation value of −23 dB.

E. PARASITIC OR SLOT ELEMENTS

Printed parasitic or slot element antennas uses two orthogonal modes [101] to create a wide impedance bandwidth by coupling either in radiating patch or in the ground plane [102]. In this technique, mutual coupling between antennas is minimized by creating extra coupling path [103], [104]. Further, one of the two coupling paths opposes the signal coming from the other coupling path, which leads to a reduction of mutual coupling. Main advantages of parasitic or slot antenna is the design simplicity, size and convenient production using either PCB technology or waveguides.

1) SQUARE-RING SLOT BASED MIMO ANTENNA

In Fig. 20, small sized mono-substrate dual polarized slot antenna is illustrated [105]. Stepped microstrip feedlines are placed perpendicular to each other. This slot behaves like a stepped impedance resonator (SIR) having a tapered profile. Middle section of the slot is kept very narrow to make the feed line coupling maximum whereas outer section is wide to achieve larger radiation aperture. The SIR slots are positioned in right angle to obtain orthogonally polarized electric fields. Further, the metallization on the top side of the substrate is used to fabricate ground plane. Four identical slots of fixed length along with stepped rectangular shape slots are etched. To improve isolation among the ports 45° tilted metallic stubs C_1 and C_2 are introduced in the junction of the arms of the ground plane. These metallic stubs blocks the spread of the electric field into the other slot arms and also restricts the spreading of ground plane current towards other ports within the antenna [106].

2) METAL STRIP REFLECTOR BASED MIMO ANTENNA

Fig. 21 comprises uniplanar two symmetric antenna elements fed through ports 1 and 2 [107]. Both antenna elements are separated by the distance of $G < 0.5\lambda_g$. Each antenna element consists of staircase-shaped radiator with a bottom shorted strip. It is observed that due to the reduced port-to-port distance there is very high mutual coupling between radiators leading towards poor isolation. Hence, to reduce mutual coupling a metal conducting strip of 0.4 mm is placed away from the feeding points at distance of $0.10 \sim 0.25\lambda_g$. This metal strip acts as a reflector and works like a coupling element between both radiating elements. Both antenna elements along with metal strip are printed on the front side of FR-4 substrate. Further, both elements are excited in their dipole mode [108]. Therefore, an enhanced isolation of −20 dB is achieved using the reflector together with the back-to-back antenna radiating elements in the UWB band.

3) STEPPED FEED-LINE AND OPEN-ENDED GROUND SLOT BASED MIMO ANTENNA

In Fig. 22, four ports open ended slot antenna is realized by creating stepped slot fed having 50 Ω microstrip line. This generates wide electric field in the opposite directions. It results negligible overlap between their impedance bandwidth [109]. Transition of resonant mode from one to another is possible due to the stepped slots of microstrip line where each slot acts like a resonating element. Length of each slot is λ/4 of its resonant frequency 5.5 GHz. The mutual coupling, in this case, is mainly reduced due to the asymmetrical structures and complementary radiation pattern without any decoupling network. The location of antenna elements (Ant_1 and Ant_2) are in a way that one radiates electric field in one direction and other in the opposite direction. Further, it is responsible for low correlation between the channels.

4) SINGLE-SHARED-RADIATING ELEMENT AND MEANDERED FEEDING LINES BASED MIMO ANTENNA

In Fig. 23, single shared radiating patch with two perpendicular meandered feeding microstrip lines are used to make MIMO antenna compact in size [110]. An open shunt stub (λ/4 length at 5.5 GHz) and a T-shaped slot are etched in the center of the radiating patch to minimize unavoidable mutual coupling. A complex connection is established from the stub

TABLE 5. Performance comparison of parasitic or slot element based MIMO antennas.

Ref.	Dimensions (mm^3) / Material	Isolation Level(dB)	Technique Employed	Gain / Radiation efficiency	ECC/DG	Application / No. of ports	Remarks
[105]	66.25× 66.25×1.6/ **FR-4**	≥ -20 dB at 3.0 ~ 12.0 GHz	Stepped feed line and square ring slots	5 ~ 8 dBi / 60%	≤ 0.005 (S-parameter)/ 9.99 dB	UWB / Dual ports	Lowest ECC
[107]	25×30×1. 6/ **FR-4**	≥ -20dB at 3.1 ~ 10.6 GHz	Two coplanar stripline-feed staircase-shaped radiating elements	5.2 dBi / 90%	= 0.1641 (S-parameter and radiation efficiency)/ 9.86 dB	UWB / Dual ports	Easy fabrication and compact size
[109]	42×25×1.6/ **FR-4**	≥ -22 dB at 3.2 ~ 12.0 GHz	Stepped-slot Feed line and open ended ground slot	4 dBi / ≤ 80%	< 0.5 (S-parameter) / 8.66 dB	Portable UWB / Quad ports	High isolation value
[110]	22×24.3×1.52/ **Rogers TMM4 60 mil**	≥ - 15 dB at 3.0 – 10.6 GHz	Meandered feed-line and stub to ground connection through Via	1.5~ 5.8dBi / 82%	< 0.42 (Far-field radiation pattern) / 9.07 dB	UWB portable devices / Dual ports	Highest gain and expensive substrate material

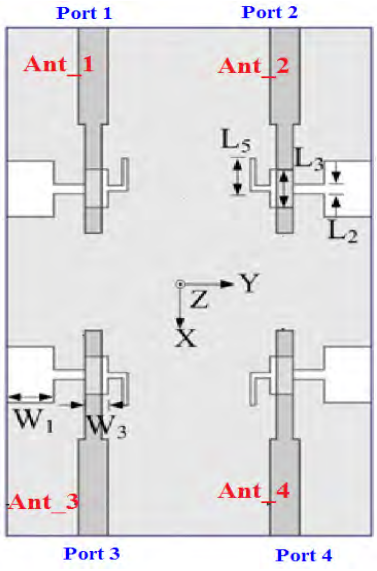

FIGURE 22. Staircase-shaped radiator and middle reflector for mutual coupling reduction [109].

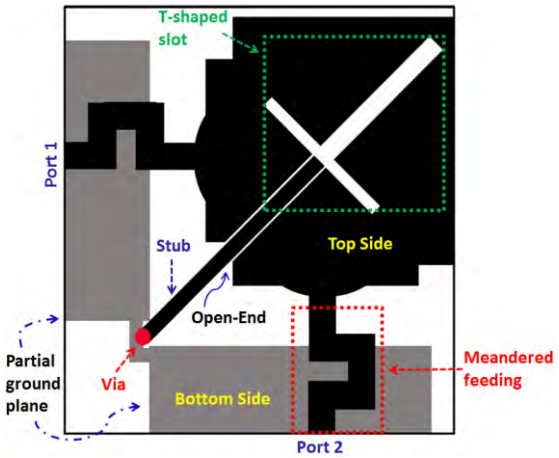

FIGURE 23. Shared radiating plane meandered feed line, slot and stub for mutual coupling reduction [110].

to the ground plane through a via. A partial ground plane of very small width is also placed on the bottom of the substrate. Meandered feedlines reduces the total distance (space diversity) from the port to radiating patch by maintaining exact 50 Ω impedance matching [111]. Excited port 1 flows the current in the radiating patch's *y*-direction and a coupled current of low magnitude appear in the *x*-direction. Further, port 2 drives the main current in *x*-direction and a lower valued coupling current are observed in *x*-direction. The orthogonal current flowing behavior makes it dual polarized in the far field.

Table 5 lists the characteristics study of parasitic or slot antennas explained in this section. The highest value of gain, bandwidth and ECC is obtained in [105]. Further, the antenna presented in [107] has highest efficiency and simple geometry.

Moreover, [109] has highest mutual coupling value of −22 dB. A novel shared radiation element structure is presented in [110].

F. RECONFIGURABLE ANTENNA

It is a switching-based technique where MEMS switches, p-i-n and varactor diodes [111], [112] are used to enhance operating frequency range and improve envelope correlation coefficients [113], [114].

1) BACK-TO-BACK MEMS SWITCHES-BASED MIMO ANTENNA

Fig. 24 shows frequency reconfigurable slot antenna consists of two back-to-back reconfigurable slots [115] using MEMS switch. The length of the slots varies from λ/4 (at 2.45 GHz)

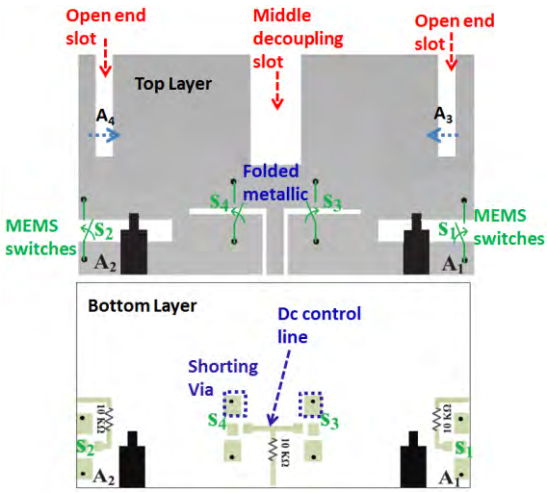

FIGURE 24. Slotted radiator MEMS-based reconfigurable antenna for mutual coupling reduction [115].

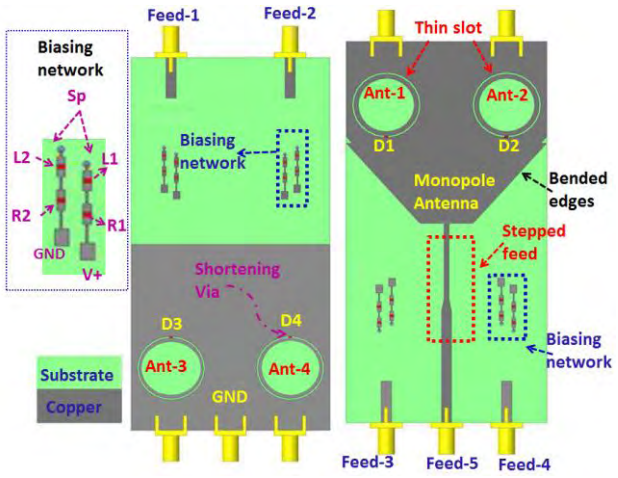

FIGURE 25. Slotted p-i-n diodes reconfigurable antenna for mutual coupling reduction [116].

to λ/2 (at 5.5 GHz) open end slots. The pair of MEMS switches is fabricated at the end of these slots.

Two compact folded metallic slots are also positioned in the middle of the substrate. It acts as a decoupling network between open ended slots A1 and A2. Moreover, it reduces the mutual coupling between those by controlling switches S3 and S4. In this design, two vertically polarized λ/4 open ended slots A3 and A4 along with middle decoupling slot are manufactured. Furthermore, it provides better isolation, decreased mutual coupling and higher bandwidth by increasing surface current distribution of the antenna. Hence, parasitic or slot element based technique is used for mutual coupling reduction.

2) SLOT-BASED P-I-N DIODES MIMO ANTENNA

Fig. 25 explains the frequency reconfigurable printed planar antenna [116]. Each side of the top and bottom plane contains two slot antenna elements. Further, it consists of a wine-glass shaped monopole antenna mentioned as Feed-5. For better impedance matching stepped feed line is used. In this case, the plane of the monopole is a dual purpose GND plane for antenna sensing applications. One side of the ground is a square plane while other has bended edges. Four circles of radius 8.5 mm has been etched out from antenna surface with very thin slot of width 0.45 mm making an outer circle of 10.1 mm radius. These thin slots help to enhance the impedance bandwidth. Further, inner circles are used for mutual coupling reduction between closely placed radiating elements. One varactor diode on each outer circle is employed and mentioned as D1, D2, D3 and D4. The connection between varactor diode and biasing network is similar as explained in [117]. Two RF inductors are connected between two terminals of the varactor diode and radiating structure to block RF signal on both end of the antenna terminals. These diodes are connected with the biasing circuit using two shortening vias. In this structure, four ports Feed-1, Feed-2, Feed-3 and Feed-4 are reconfigurable and one Feed-5 is traditional UWB sensing antenna. All the antenna elements are analogous in structures and symmetrically placed on the substrate.

3) PLANAR INVERTED-F P-I-N DIODES BASED MIMO ANTENNA

In Fig. 26, the MIMO antenna consists of two symmetrically identical planar inverted-F antenna (PIFA) radiators where two diodes D_1 and D_2 are connected [118] to make it reconfigurable. Each PIFA radiator is connected to the ground plane through a shorting plate and vertical feed line. A λ/4 length at 2.35 GHz slot line (Ls) is also implanted in the ground plane between both radiating elements. Two more switching p-i-n diodes (D_3 and D_4) are positioned on this slot length to provide better isolation at three different operating frequencies 2.3 ∼ 2.4 GHz, 2.5 ∼ 2.7 GHz and 3.4 ∼ 3.6 GHz. It is known as DGS technique for mutual coupling reduction. By controlling the length Ls the state of the PIN diode's operational mode can be changed. DC biasing is provided to D_1 and D_2 through RF inductor to prevent RF signal leakage. Further, the DC biasing of D_3 and D_4 is provided by the coupling capacitors C_1 and C_2, respectively. By varying the capacitance values the isolation characteristics can be controlled which also can control the mutual coupling properties.

4) MICROSTRIP LOOP AND SLOT FREQUENCY RECONFIGURABLE-BASED MIMO ANTENNA

Fig. 27 shows the dual frequency band reconfigurable microstrip printed loop antenna and slot antenna [119]. Upper side of the substrate is used for ground as well as radiating patch structure. The left side of the antenna consists of an L-shaped microstrip section named as Antenna # 1. It has stepped slot and shortening line for impedance matching which is excited by L-shaped microstrip. However, its right side consists of microstrip loop antennas (Antenna #2 and Antenna #3), PIN diode switches and biasing network.

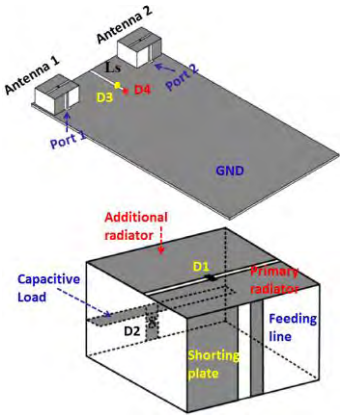

FIGURE 26. Inverted F PIN diodes reconfigurable for mutual coupling reduction [118].

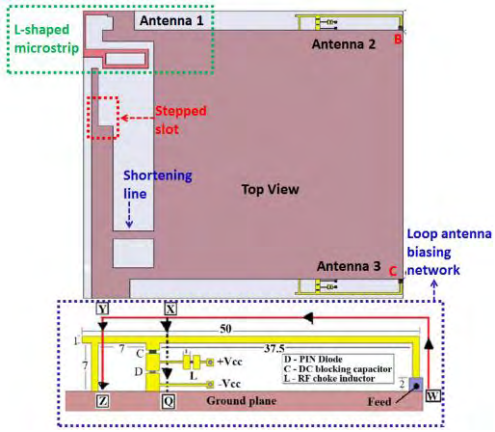

FIGURE 27. Microstrip loop and slot reconfigurable antenna for mutual coupling reduction [119].

Depending upon the on and off state of the switches two resonating paths are achieved. Switch off state resonates W-X-Y-Z path provides long term evaluation (LTE) frequency band (1.6 $\sim$ 1.9 GHz). Further, switch on state resonance path is W-Q-Z provides industrial scientific and medical (ISM) frequency band (2.2 $\sim$ 2.94 GHz). A shortening line and stepped slot (parasitic or slot element technique) is used for mutual coupling reduction. Moreover, the antenna is greatly affected by the lengths of the biasing components. Therefore, a 20 pF capacitor is used to stop DC signals to the RF input of the loop antennas. A high value inductor in series with 47 Ω resistance is used for PIN diode biasing. This biasing network also helps in mutual coupling reduction.

Table 6 lists the characteristics of frequency reconfigurable antenna explained in section IV.F. The MIMO antenna structure explained in [118] is complex due to the shorting plate and vertical adjusted feed line. It has lowest value of ECC and maximum diversity gain [120]. Further, it has lowest mutual coupling value of −47dB compared to other antennas in this section. However, [119] shows maximum efficiency of 92% and maximum gain of 5 dBi.

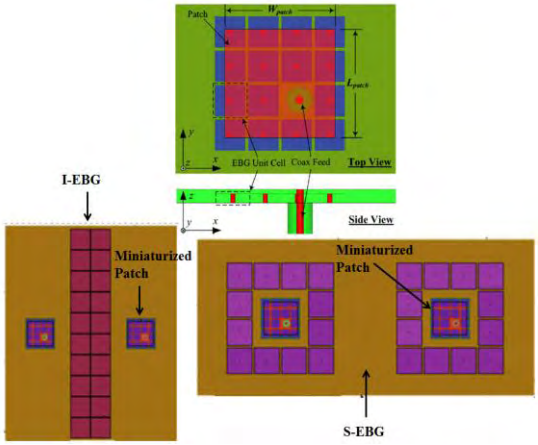

FIGURE 28. I and S mushroom-based EBG for mutual coupling reduction [124].

G. ELECTROMAGNETIC BANDGAP STRUCTURE

Electromagnetic bandgap (EBG) structure can block electromagnetic waves of specific frequency or acts as a medium to transmit electromagnetic waves [121]. Depending on the field of application different stop band, pass band and bandgap frequencies can be identified [122]. This structure is a periodic arrangement of metallic or dielectric material. Periodicity in the structure and individual resonance of the elements can generate multiple band gaps [123].

1) MUSHROOM-TYPE EBG BASED MIMO ANTENNA

Fig. 28 shows probe feed patch antenna on the EBG substrate [124]. It introduces parasitic capacitance and inductance. Therefore, the phase constant of an EM wave propagating underneath the radiating patch is larger than transverse electromagnetic (TEM) mode. Consequently, EBG structure works in a slow wave region with wavelength shorter than TEM mode. Traditionally, EBG element is placed between the antenna elements. However, for mutual coupling reduction antenna element is surrounded by the EBG elements. There are two ways to arrange open mushroom-type EBG structure between antenna elements. One is by surrounding each radiating patch with square ring of EBG cells which is known as S-EBG configuration. Another is the placement of any array of EBG cells between two radiating patches known as I-EBG structure. Highest isolation is observed in case of S-EBG structure cell arrangement as it reduces inter-element coupling. Hence, four-port S-EBG structure antenna arrangement with improved front to back lobe ratio is achieved.

2) DUAL LAYER MULTI-ELEMENT EBG-BASED MIMO ANTENNA

Fig. 29 shows dual layer mushroom EBG structure- based on slow wave propagation [125]. The lower layer of the mushroom EBG works with low frequency waves of 2.45 GHz. Further, upper layer acts as a band stop filter at 2.55 GHz resonant frequency. The mushroom layer is manufactured on

TABLE 6. Performance comparison of frequency reconfigurable based MIMO antennas.

Ref.	Dimensions (mm^3) / Material	Isolation Level(dB)	Technique Employed	Gain / Radiation efficiency	ECC/DG	Application / No. of ports	Remarks
[115]	46× 20×1.6/ **FR-4**	≥ -18 dB at 2.39 ~ 2.48GHz and 5.15 ~ 6.4 GHz (Off state) ≥ -14.5 dB at 5 ~ 6.1GHz (On state)	RF MEMS Switches	2.9 dBi / 83%	≤ 0.2 (S-Parameter and Radiation Efficiency) / 9.89 dB	WLAN / Quad ports	Complex geometry
[116]	120×60×1.5/ **RO-4350**	≥ -12 dB at 1.77 ~ 2.51 GHz ≥ -25 dB at 0.75 ~ 7.65GHz	One varactor Diodes per element and biasing circuit	0.5 ~ 3.2 dBi /65 ~ 81 %	0.079 ~ 0.082 (Far-Field Radiation pattern) / 9.96 ~ 9.95 dB	UWB and Cognitive Radio (CR) / Five ports	Complex geometry and expensive material
[118]	90×50×0.8/ **FR-4**	≥ -47 dB at 2.3 ~ 2.4GHz for (D_1 , D_2 On state) , ≥ -30.8 dB at 3.4 ~ 3.6 GHz for (D_3 On state) , ≥ - 43 dB at 2.5 ~ 2.7GHz for (D_1 , D_4 On state)	Two Pin diodes and DC biasing circuit	1.99 ~ 2.78 dBi / 48.43 ~ 73.1 %	≤ 0.0056~ 0.110 (Far-Field Radiation pattern)/ 9.42~ 9.97 dB	WiMax / Quad ports	Lowest ECC and mutual coupling
[119]	150×150×0.8/ **FR-4**	≥ -20 dB at 1.6 ~ 1.9 GHz (Off state) ≥ -20 dB at 2.2 ~ 2.96 GHz (On state)	Two Pin diodes switches and biasing network	3~5 dBi / 55 – 83 % (Lower band) 75 – 92 % (upper band)	Off state < 0.25(S-Parameter) / 9.68 dB On state < 0.09 (S-Parameter) / 9.95 dB	LTE and portable wireless DTV media players / triple ports	Highest efficiency and maximum gain

the top of the substrate. Two layers of the substrate are used to increase the antenna resonance frequency by lowering down the effective dielectric constant. In lower layers, EBG unit cells are arranged in square grid-like pattern which is known as matrix arrangement. Additionally, the upper layer EBG unit cells (5×2) are arranged in the linear structure. The upper mushroom cells are used to reduce mutual coupling.

3) PERIODIC Z-SHAPED EBG BASED MIMO ANTENNA

In Fig. 30, a planner compact antenna with unique feature of wide-angle scanning is presented [126]. Eight EBG cell elements are arranged in two columns between microstrip square patches to reduce mutual coupling. The square radiating patches are fed by the co-axial probes. The proposed EBG has periodic distribution of Z-shaped etched metallic elements. Further, this structure has periodic boundary conditions with appropriate phase shifts.

4) ONE DIMENSIONAL AND SPLIT RING RESONATOR EBG BASED MIMO ANTENNA

Fig. 31 shows hybrid antenna technique to suppress mutual coupling. One dimensional (1-D) electromagnetic bandgap and split ring resonator (SRR) structure [127] has been

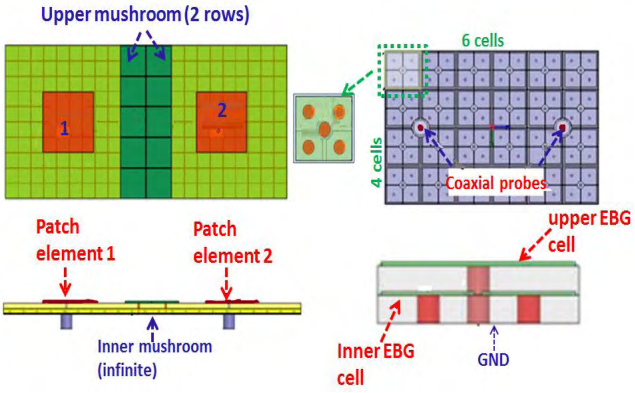

FIGURE 29. Dual layer multi-element based on EBG for mutual coupling reduction [125].

inserted between two radiating elements. The SRR acts as a reflector and wave trap. Further, EBG structure blocks these waves to improve antenna performance. This 1-D EBG is constructed by eight periodic cells patterned in columns. Each unit cell has an interdigitated capacitor and meander lines. Moreover, the addition of SRR improves the reflection phase from 30° to 90° (quadratic phase) and provides better

TABLE 7. Performance comparison of electromagnetic bandgap based MIMO antennas.

Ref.	Dimensions (mm^3) / Material	Isolation Level(dB)	Technique Employed	Gain / Radiation efficiency	ECC/DG	Application / No. of ports	Remarks
[124]	95×95×2.284/ **Rogers RO4350B**	≥ -25 dB at 2.395 ~2.42 GHz	S-EBG and Vias	5.12dBi / 56.57%	NG /NG	ISM / Quad ports	Complex geometry
[125]	35×40×1.6/ **FR-4**	≥ -28 dB at 2.45 ~2.55 GHz	Dual layer Mushroom EBG structures	4.55 ~ 4.92 dBi / 64.42 ~ 66.94 %	= 0.01(S-Parameter and Radiation Efficiency)/ 9.9 dB	ISM/ Dual ports	Extremely complex geometry and small size
[126]	90×45×1.6/ **FR-4**	≥ -30.35 dB at 5.59GHz	8 Z-shaped etched EBG structure in 2 columns	2.42dB / NG	NG /NG	WLAN/ Dual ports	Simple geometry and large size
[127]	60×57×1.2/ **FR-4**	≥ -53.7dB at 2.43 ~ 2.54 GHz	1 dimensional EBG and Split ring resonator (SRR)	NG / 82%	0.002 (Far-Field Radiation pattern)/9.98 dB	ISM / Dual ports	Simple geometry and high efficiency

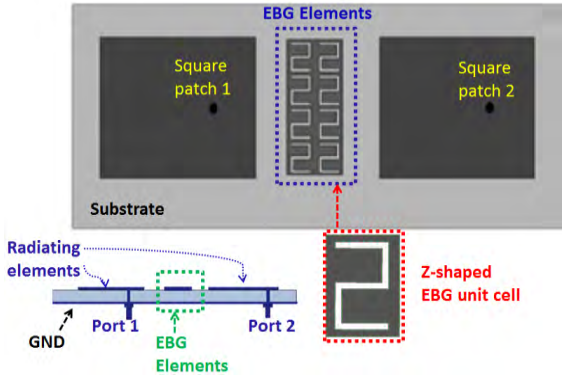

FIGURE 30. Periodic Z-shaped based on EBG for mutual coupling reduction [126].

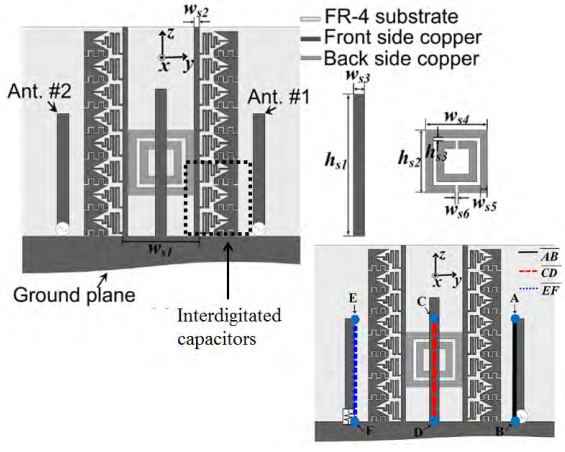

FIGURE 31. One dimensional and split ring resonator EBG for mutual coupling reduction [127].

impedance matching. Near field coupling is observed using imaginary lines of AB, CD and EF located 1mm higher on the pattern structure for mutual coupling path observation. Sudden phase change with respect to frequency exhibits 1-D EBG and SRR to maintain waves in certain direction. This contributes in mutual coupling reduction at different frequencies.

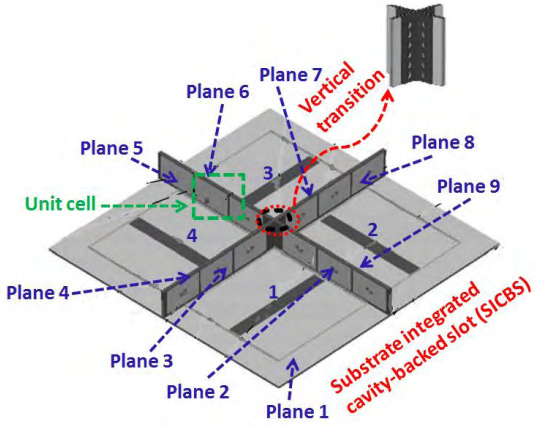

FIGURE 32. One dimensional and split ring resonator EBG for mutual coupling reduction [131].

Table 7 lists an overview of electromagnetic bandgap technique-based MIMO antennas presented in this section.

Compared to other structures [126] has simplest geometry, easy fabrication. Additionally, the lowest mutual coupling of −53.7 dB is obtained. Further, [127] has highest efficiency using a hybrid structure of SRR and EBG.

H. METAMATERIALS ANTENN

In this antenna design technique, the MIMO configurations are fabricate by assembling composite materials; such as metals and plastics. The repeating pattern of the materials makes it capable of manipulating EM waves. Similarly, meta-surface [128]–[130] equivalent to a negative permeability medium is also used as metamaterial in mutual coupling reduction in MIMO antenna system [145], [146].

1) SUBSTRATE INTEGRATED CAVITY DOUBLE LAYER MUSHROOM-BASED MIMO ANTENNA

Fig. 32 presents orthogonally distributed compact four element substrate integrated cavity-backed slot (SICBS) antenna systems consist of double layer mushroom structure [131].

TABLE 8. Performance comparison of metamaterials based MIMO antennas.

Ref.	Dimensions (mm3) / Material	Isolation Level(dB)	Technique Employed	Gain / Radiation efficiency	ECC/DG	Application / No. of ports	Remarks
[131]	119×119×22.5/ **Rogers RO4003, RO4450B**	≥ -42 dB at 2.395 – 2.45 GHz	Four element SICBS	NG / NG	<0.02(Far-Field Radiation pattern)/ 9.89 dB	ISM / Quad ports	Complex geometry and large size
[132]	26×29.3×1.6/ **FR-4**	≥ -28 dB at 5.55 GHz	Cascaded transmission line and vias	NG / 66.94 %	0.01(S-parameter)/9.97 dB	WLAN / Dual ports	Simple geometry
[133]	22×5×5/ **FR-4**	≥ -15dB at 4.55 ~ 4.75 GHz	2 triangular layers of metal and foam	NG / 77%	NG/NG	Mobile Handset / Dual ports	Smallest size and complex geometry

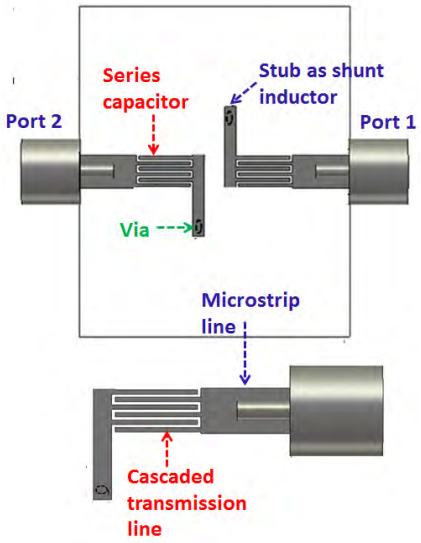

FIGURE 33. Cascaded transmission line based on metamaterials for mutual coupling reduction [132].

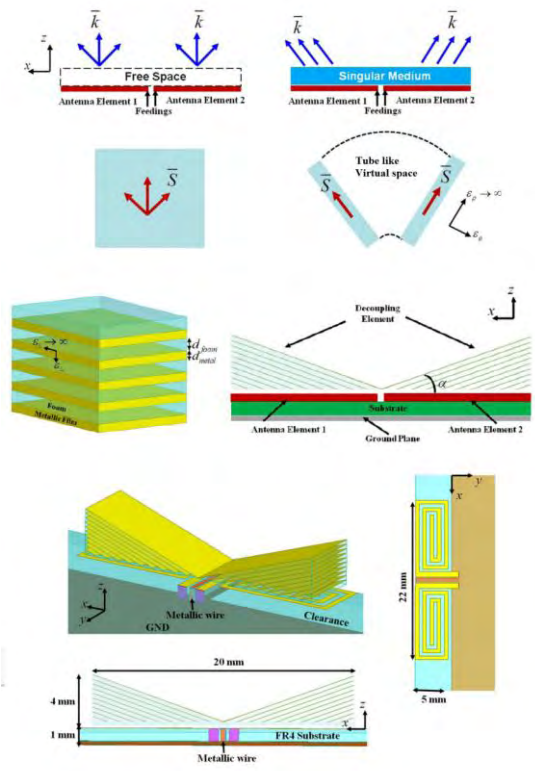

FIGURE 34. Deep-subwavelength metamaterials antenna for mutual coupling reduction [133].

To improve isolation between antenna elements a wall with double layer mushroom structure (EBG technique) is applied. Four pieces of double layer mushroom walls are orthogonally crossed on top of the antenna elements. This double layer mushroom cell is made of two layer substrate of same thickness. Two identical patches are etched on the top of upper substrate and bottom of lower substrate, respectively. There is a ground sandwiched between two substrates. Further, a via of fix diameter is used to connect both patches to the ground plane. The isolation between antenna elements is the function of height of the double layer mushrooms.

2) CASCADED TRANSMISSION LINE METAMATERIAL-BASED MIMO ANTENNA

Reversal composite right-left-handed (CRLH) configuration MIMO antenna using metamaterial [132] is shown in Fig. 33. By cascading metamaterial transmission line in this configuration both stub and interdigital capacitors can be reversed. Hence, by reversing the unit cell of cascaded transmission line the current induced inside antenna element can be reversed. This helps in mutual coupling reduction and high isolation achievement.

3) DEEP-SUBWAVELENGTH METAMATERIALS-BASED MIMO ANTENNA

Fig. 34 shows metamaterials-based decoupling strategy adopted antenna [133]. Singular medium is made of subwavelength metal and air layers. In this work, alternating metallic and dielectric layers are composed to form a singular medium.

TABLE 9. Performance comparison of decoupling networks MIMO antennas.

Ref.	Dimensions (mm^3) / Material	Isolation Level(dB)	Technique Employed	Gain / Radiation efficiency	ECC/DG	Application / No. of ports	Remarks
[141]	72.4×20×0.8/ **Rogers RO4350B**	≥ -27.6dB at 2.18 ~2.65 GHz	Diamond-shaped patterned ground resonator	1.39dBi / 66 ~70.5%	0.08 ~ 0.09 (Far-Field Radiation pattern) / 9.96 ~ 9.95 dB	ISM / Dual ports	Medium size and complex geometry
[142]	70×35×0.8/ **FR-4**	≥ -32dB at 3.45 ~ 3.55 GHz	Reactive dummy loads	NG / 82%	0.16 ~ 0.19 (Far-Field Radiation pattern)/ 9.87 ~ 9.81 dB	WiMAX / Triple ports	Simple geometry
[143]	112×55×1.6/ **FR-4**	≥ -15 dB at 2.4 ~2.48 GHz and ≥ -15dB at 5.15 ~ 5.35 GHz	Coupled resonator decoupling network (CDRN)	NG / 66 ~ 75%	0.23 ~ 0.13 at 2.45 GHz ,0.04 ~ 0.008 at 5.25 GHz (Far-Field Radiation pattern)/ 9.73 ~ 9.99 dB	ISM and WLAN / Dual ports	Large dimensions and Dual band
[144]	40×100×0.8/ **FR-4**	≥ -15dB at 3.5~ 3.6 GHz	Pattern diversity decoupling network	NG / 50%	> 0.15 (Far-Field Radiation pattern)/ 9.88 dB	WiMAX / Eight ports	Maximum ports and simple geometry

Two antenna elements are located closely where the EM wave's energy spread out due to different permittivity elements. Hence, radiated waves can propagate along the radial direction and corresponding flow of energy is confined in tube-like virtual space. Two triangular layered structures with an oblique angle between their surfaces along with a decoupling matrix are designed in the ground. A square metallic wire of 1 mm is also inserted between two antennas in the substrate to prevent unnecessary scattering of energy within the substrate. This technique is used to reduce mutual coupling. To avoid surface current interference leading to higher mutual coupling the antenna pair is not located on the midpoint of the ground edges. The singular medium is effective for lower dispersion, maximum anisotropy and fewer losses. This quality does not affect MIMO antenna efficiency and improves isolation in the broadband range.

Table 8 shows [131] has complex geometry and lowest mutual coupling of −42 dB compared to other antennas presented in this section. Whereas, [132] has simplest geometry with lowest ECC value.

I. DECOUPLING NETWORKS

Decoupling networks [134], [135] are used to achieve better isolation in the MIMO antenna systems. This works on the principle of transformation of cross-admittance term to purely imaginary value by adding transmission lines or by discrete components. Eigen mode decomposition [136], artificial structure [137], coupled resonator [138] and inserted components [139], [140] are some of the decoupling schemes.

1) DSPRG- PLANE DECOUPLING NETWORK

Fig. 35 shows dual port MIMO antenna consists of two symmetrical L-shaped inverted-F antenna elements as radiator of

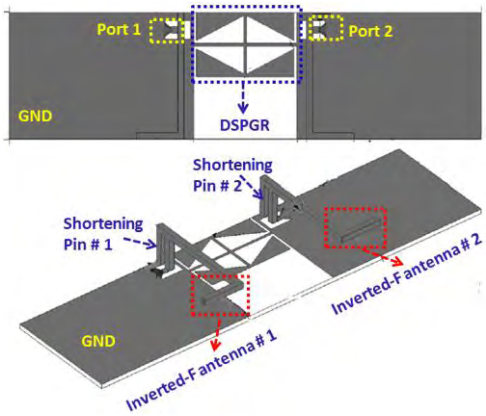

FIGURE 35. Diamond-shaped pattern grounds resonator based decoupling structure for the reduction of mutual coupling [141].

height 6 mm [141]. In this work, the ground has diamond shaped pattern which acts as a resonator. This is known as diamond-shaped patterned ground resonator (DSPRG). It also works as a decoupling element. It can reduce mutual coupling in the wideband by suppressing the surface current in the antenna elements of MIMO antenna.

2) DUMMY LOAD-BASED DECOUPLING NETWORKS

Fig. 36 shows a new technique presented in [142]. In this work, higher isolation is achieved by introducing a pair of dummy elements terminated with reactive loads. This method relies only on antenna impedance. The admittances of both dummy loads are closed to each other. Simple three port monopole antennas are printed on top of the substrate by 0.15λ distance between them. Without dummy loads there is very poor isolation and impedance mismatch. A reactive load used as dummy element is realized by distributed or

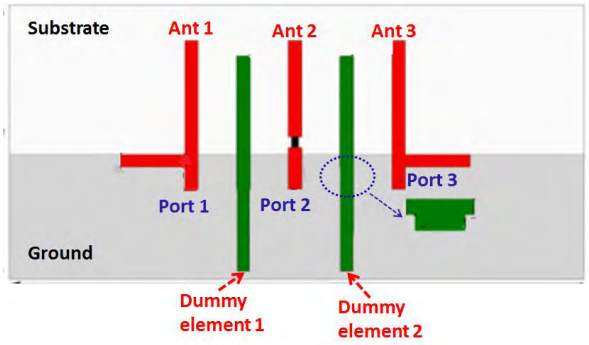

FIGURE 36. Dummy load based decoupling structure for the reduction of mutual coupling [142].

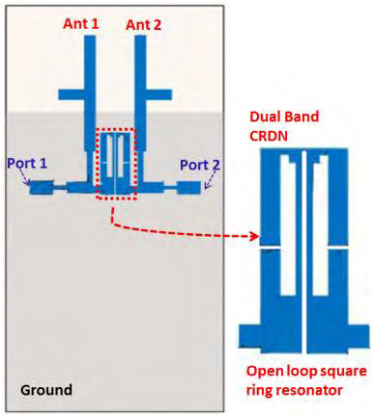

FIGURE 37. Dual band coupled resonator based decoupling structure for mutual coupling [143].

lumped elements. Furthermore, tuning is established using two open circuited transmission lines.

3) COUPLED RESONATOR DECOUPLING NETWORK

In Fig. 37, coupled resonator decoupling network (CDRN) [143] is applied to reduce the mutual coupling between two dual band antennas. This decoupling network consists of a pair of open loop square ring resonator. CDRN is considered as lossless passive networks for dual band application.

4) MULTI-ELEMENT PATTERN DIVERSITY BASED DECOUPLING NETWORK

Fig. 38 shows planner monopole MIMO antenna-based on pattern diversity decoupling method [144]. In this work, radiation pattern is maintained by changing length of the radiator. The antenna's radiation pattern is affected by the electrical length and other parameters; such as the ground plane dimension, radiator shape and substrate material. To achieve high isolation antenna radiators are placed in close vicinity. It alters near field radiation of the antenna to reduce mutual coupling. Two identical set of 4-element MIMO antennas are symmetrically arranged on edges of the substrate. Four top-hat antennas are closer to the side edges of the ground plane as compared to inverted L-shaped ones. For impedance

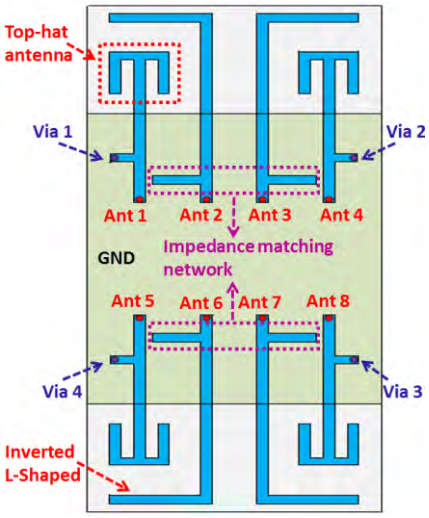

FIGURE 38. Multi-element pattern diversity based decoupling structure for mutual coupling [144].

matching realization a stub is added to the feeding line of Ant 2, Ant 3, Ant 6 and Ant 7. Dimension of both radiators and impedance matching network required fine tuning for better isolation.

Table 9 compares different MIMO antenna characteristics using decoupling network. In [142], highest efficiency and lowest mutual coupling of −32 dB are achieved using simplest geometry of dummy loads. Further, [143] shows dual band operation. It also achieves lowest ECC value of 0.008.

V. CONCLUSION

This review work describes every mutual coupling reduction techniques considered for MIMO antenna design present in the literature. To understand the critical feature of a particular technique, multiple examples are adopted. Comparison on the basis of dimensions, materials, gain, ECC, diversity gain and radiation efficiency is presented for all the MIMO antenna techniques. The minimum requirement for mutual coupling adopted by the most of the researchers is −17dB to −20 dB. The values lower than this contributes to the alteration of the self- and mutual-impedances of the MIMO antenna systems therefore, affects the antenna mismatches and embedded radiation efficiencies. In this paper, unique isolation techniques employed by the researchers to achieve higher isolation and lower ECC is the key comparison element. This review work demonstrates that by using DGS and CSRR technique very wide band of frequency can be achieved in MIMO with lower correlation values. Further, the straight neutralization lines offer simple structure with a significantly improved isolation. Parasitic or slot element makes the antenna compact in size with improved ECC and efficiency. Similarly, EBG architecture consists of complex periodic arrangement of metallic or dielectric structure at the cost of lower bandwidth. Furthermore, decoupling networks offer simple geometry with better performance. DRA is area inefficient and complex compared to printed antennas.

Moreover, reconfigurable and metamaterial-based antennas provide higher performance at the cost of expensive manufacturing procedure. Mutual coupling reduction is an important area of research which can have a direct impact for the development of the next generation wireless communication systems, such as 5G, 6G and massive MIMO. Therefore, a wide range of design possibilities is presented in this work to enlighten the improvement of the mutual coupling which is rare in the literature. Thus, this work can provide a broad overview to the early stage and specialist antenna designers about different isolation techniques as a thorough reference for the research field of recent MIMO antennas.

REFERENCES

[1] C. Oestges, M. Guillaud, and M. Debbah, "Multi-polarized MIMO communications: Channel model, mutual information and array optimization," in *Proc. IEEE Wireless Commun. Netw. Conf.*, Mar. 2007, pp. 1057–1061.

[2] M. Sánchez-Fernández, E. Rajo-Iglesias, Ó. Quevedo-Teruel, and M. L. Pablo-González, "Spectral efficiency in MIMO systems using space and pattern diversities under compactness constraints," *IEEE Trans. Veh. Technol.*, vol. 57, no. 3, pp. 1637–1645, May 2008.

[3] L. Wang, G. Wang, and Q. Zhao, "Suppressing mutual coupling of MIMO antennas with parasitic fragment-type elements," in *Proc. 46th Eur. Microw. Conf. (EuMC)*, 2016, pp. 1303–1306.

[4] X. Wang, Z. Feng, and K. M. Luk, "Pattern and polarization diversity antenna with high isolation for portable wireless devices," *IEEE Antennas Wireless Propag. Lett.*, vol. 8, pp. 209–211, 2009.

[5] A. J. Paulraj, D. A. Gore, R. U. Nabar, and H. Bolcskei, "An overview of MIMO communications—A key to gigabit wireless," *Proc. IEEE*, vol. 92, no. 2, pp. 198–218, Feb. 2004.

[6] R. G. Vaughan and J. B. Andersen, "Antenna diversity in mobile communications," *IEEE Trans. Veh. Technol.*, vol. VT-36, no. 4, pp. 149–172, Nov. 1987.

[7] M. Rumney, "Design and verification challenges," in *LTE and the Evolution to 4G Wireless—Design and Measurement Challenges*. Hoboken, NJ, USA: Wiley, 2013.

[8] A. Stjernman, "Relationship between radiation pattern correlation and scattering matrix of lossless and lossy antennas," *Electron. Lett.*, vol. 41, no. 12, pp. 678–680, Jun. 2005.

[9] K. Wei, J.-Y. Li, L. Wang, and R. Xu, "Microstrip antenna array mutual coupling suppression using coupled polarisation transformer," *IET Microw., Antennas Propag.*, vol. 11, no. 13, pp. 1836–1840, Jul. 2017.

[10] T. Hall *et al.*, "Non-contact sensor for long-term continuous vital signs monitoring: A review on intelligent phased-array Doppler sensor design," *Sensors*, vol. 17, no. 11, p. 2632, Nov. 2017.

[11] L. H. Trinh, F. Ferrero, L. Lizzi, J.-M. Ribero, and R. Staraj, "4×4 MIMO multiband antenna system for mobile handsets," *Int. J. Antennas Propag.*, vol. 2015, Nov. 2015, Art. no. 857876.

[12] M. S. Sharawi, "Printed multi-band MIMO antenna systems: Techniques and Isolation mechanisms," in *Proc. 8th Eur. Conf. Antennas Propag. (EuCAP)*, 2014, pp. 779–783.

[13] H.-C. Huang, "Overview of antenna designs and considerations in 5G cellular phones," in *Proc. Int. Workshop Antenna Technol. (iWAT)*, 2018, pp. 1–4.

[14] Z. Ying, "Antennas in cellular phones for mobile communications," *Proc. IEEE*, vol. 100, no. 7, pp. 2286–2296, Jul. 2012.

[15] P.-Y. Qin, Y. J. Guo, and C.-H. Liang, "Effect of antenna polarization diversity on MIMO system capacity," *IEEE Antennas Wireless Propag. Lett.*, vol. 9, pp. 1092–1095, Nov. 2010.

[16] M. S. Sharawi, A. B. Numan, and D. N. Aloi, "Isolation improvement in a dual-band dual-element mimo antenna system using capacitively loaded loops," *Prog. Electromagn. Res.*, vol. 134, pp. 247–266, 2013.

[17] H. S. Lui and H. T. Hui, "Mutual coupling compensation for direction-of-arrival estimations using the receiving-mutual-impedance method," *Int. J. Antennas Propag.*, vol. 2010, Jan. 2010, Art. no. 373061.

[18] Y. Wu, J. W. M. Bergmans, and S. Attallah, "Effects of antenna correlation and mutual coupling on the carrier frequency offset estimation in MIMO systems," in *Proc. 6th Int. Conf. Wireless Commun. Netw. Mobile Comput. (WiCOM)*, 2010, pp. 1–4.

[19] B. Wang, Y. Chang, and Y. Sun, "Performance of the large-scale adaptive array antennas in the presence of mutual coupling," *IEEE Trans. Antennas Propag.*, vol. 64, no. 6, pp. 2236–2245, Jun. 2016.

[20] D. M. Pozar, "A relation between the active input impedance and the active element pattern of a phased array," *IEEE Trans. Antennas Propag.*, vol. 51, no. 9, pp. 2486–2489, Sep. 2003.

[21] K.-H. Chen and J.-F. Kiang, "Effect of mutual coupling on the channel capacity of MIMO systems," *IEEE Trans. Veh. Technol.*, vol. 65, no. 1, pp. 398–403, Jan. 2016.

[22] X. Chen, S. Zhang, and A. Zhang, "On MIMO-UFMC in the presence of phase noise and antenna mutual coupling," *Radio Sci.*, vol. 52, no. 11, pp. 1386–1394, 2017.

[23] L. Sun, P. Li, M. R. McKay, and R. D. Murch, "Capacity of MIMO systems with mutual coupling: Transmitter optimization with dual power constraints," *IEEE Trans. Signal Process.*, vol. 60, no. 2, pp. 848–861, Feb. 2012.

[24] H. T. Hui, K. Y. Chan, and E. K. N. Yung, "Compensating for the mutual coupling effect in a normal-mode helical antenna array for adaptive nulling," *IEEE Trans. Veh. Technol.*, vol. 52, no. 4, pp. 743–751, Jul. 2003.

[25] C. Knievel and P. A. Hoeher, "On particle swarm optimization for MIMO channel estimation," *J. Elect. Comput. Eng.*, vol. 2012, Dec. 2012, Art. no. 614384.

[26] N. Sindhwani, M. S. Bhamrah, A. Garg, and D. Kumar, "Performance analysis of particle swarm optimization and genetic algorithm in MIMO systems," in *Proc. 8th Int. Conf. Comput., Commun. Netw. Technol. (ICCCNT)*, 2017, pp. 1–6.

[27] A. Recioui and H. Bentarzi, "Genetic algorithm based MIMO capacity enhancement in spatially correlated channels including mutual coupling," *Wireless Pers. Commun.*, vol. 63, no. 3, pp. 689–701, 2012.

[28] A. Recioui and H. Bentarzi, "Capacity optimization of MIMO wireless communication systems using a hybrid genetic-Taguchi algorithm," *Wireless Pers Commun*, vol. 71, no. 2, pp. 1003–1019, Jul. 2013.

[29] A. Recioui, "Application of a galaxy-based search algorithm to MIMO system capacity optimization," *Arabian J. for Sci. Eng.*, vol. 41, no. 9, pp. 3407–3414, 2016.

[30] H. Wei, D. Wang, H. Zhu, J. Wang, S. Sun, and X. You, "Mutual coupling calibration for multiuser massive MIMO systems," *IEEE Trans. Wireless Commun.*, vol. 15, no. 1, pp. 606–619, Jan. 2016.

[31] H. Singh, H. L. Sneha, and R. M. Jha, "Mutual coupling in phased arrays: A review," *Int. J. Antennas Propag.*, vol. 2013, Mar. 2013, Art. no. 348123.

[32] C. Craeye and D. González-Ovejero, "A review on array mutual coupling analysis," *Radio Sci.*, vol. 46, no. 2, pp. 1–25, 2011.

[33] X. Zhu, X. Yang, Q. Song, and B. Lui, "Compact UWB-MIMO antenna with metamaterial FSS decoupling structure," *J. Wireless Commun. Netw.*, vol. 2017, no. 1, p. 115, Dec. 2017.

[34] Y. Ou, X. Cai, and K. Qian, "Two-element compact antennas decoupled with a simple neutralization line," *Prog. Electromagn. Res.*, vol. 65, pp. 63–68, 2017.

[35] M. Bilal, R. Saleem, H. H. Abbasi, M. F. Shafique, and A. K. Brown, "An FSS-based nonplanar quad-element UWB-MIMO antenna system," *IEEE Antennas Wireless Propag. Lett.*, vol. 16, pp. 987–990, 2017.

[36] M. S. Khan, A.-D. Capobianco, S. M. Asif, D. E. Anagnostou, R. M. Shubair, and B. D. Braaten, "A compact CSRR-enabled UWB diversity antenna," *IEEE Antennas Wireless Propag. Lett.*, vol. 16, pp. 808–812, 2017.

[37] M. A. Abdalla and A. A. Ibrahim, "Design and performance evaluation of metamaterial inspired MIMO antennas for wireless applications," *Wireless Pers. Commun.*, vol. 95, no. 2, pp. 1001–1017, 2017.

[38] Y.-S. Chen and C.-P. Chang, "Design of a four-element multiple-input–multiple-output antenna for compact long-term evolution small-cell base stations," *IET Microw., Antennas Propag.*, vol. 10, no. 4, pp. 385–392, 2016.

[39] S. Chouhan, D. K. Panda, M. Gupta, and S. Singhal, "Multiport MIMO antennas with mutual coupling reduction techniques for modern wireless transreceive operations: A review," *Int. J. RF Microw. Comput.-Aided Eng.*, vol. 28, no. 2, p. e21189, Feb. 2018.

[40] M. S. Sharawi, A. T. Hassan, and M. U. Khan, "Correlation coefficient calculations for MIMO antenna systems: A comparative study," *Int. J. Microw. Wireless Technol.*, vol. 9, no. 10, pp. 1991–2004, 2017.

[41] S. Shrestha, S.-K. Noh, and D.-Y. Choi, "Comparative study of antenna designs for RF energy harvesting," *Int. J. Antennas Propag.*, vol. 2013, Jan. 2013, Art. no. 385260.

[42] X. Chen, S. Zhang, and Q. Li, "A review of mutual coupling in MIMO systems," *IEEE Access*, vol. 6, pp. 24706–24719, 2018.
[43] J. L. Allen and B. L. Diamond, "Mutual coupling in array antennas," Massachusetts Inst. Technol. Lincoln Lab., Lexington, MA, USA, Tech. Rep. TR-424, Oct. 1966.
[44] L. Malviya, R. K. Panigrahi, and K. Machavaram, "MIMO antennas with diversity and mutual coupling reduction techniques: A review," *Int. J. Microw. Wireless Technol.*, vol. 9, no. 8, pp. 1763–1780, 2017.
[45] L. Savy and M. Lesturgie, "Coupling effects in MIMO phased array," in *Proc. IEEE Radar Conf. (RadarConf)*, May 2016, pp. 1–6.
[46] H. T. Hui, M. E. Bialkowski, and H. S. Lui, "Mutual coupling in antenna arrays," *Int. J. Antennas Propag.*, vol. 2010, Feb. 2010, Art. no. 715138.
[47] X. Chen, "Antenna correlation and its impact on multi-antenna system," *Prog. Electromagn. Res. B*, vol. 62, pp. 241–253, Jan. 2015.
[48] M. Manteghi and Y. Rahmat-Samii, "Multiport characteristics of a wideband cavity backed annular patch antenna for multipolarization operations," *IEEE Trans. Antennas Propag.*, vol. 53, no. 1, pp. 466–474, Jan. 2005.
[49] S. H. Chae, W. I. Kawk, S.-O. Park, and K. Lee, "Analysis of mutual coupling in MIMO antenna array by TARC calculation," in *Proc. Asia–Pacific Microw. Conf.*, 2006, pp. 2090–2093.
[50] M. A. Matin, *Wideband, Multiband, and Smart Reconfigurable Antennas for Modern Wireless Communications*, 1st ed. Hershey, PA, USA: IGI Global, 2015.
[51] S. Stein, "On cross coupling in multiple-beam antennas," *IRE Trans. Antennas Propag.*, vol. 10, no. 5, pp. 548–557, Sep. 1962.
[52] Z. Ying, C.-Y. Chiu, K. Zhao, S. Zhang, and S. He, "Antenna design for diversity and MIMO application," in *Handbook of Antenna Technologies*. Singapore: Springer, 2015, pp. 1–43.
[53] G. Tsoulos, *MIMO System Technology for Wireless Communications*. Boca Raton, FL, USA: CRC Press, 2006.
[54] H. Li, X. Lin, B. K. Lau, and S. He, "Equivalent circuit based calculation of signal correlation in lossy MIMO antennas," *IEEE Trans. Antennas Propag.*, vol. 61, no. 10, pp. 5214–5222, Oct. 2013.
[55] P. Hallbjorner, "The significance of radiation efficiencies when using S-parameters to calculate the received signal correlation from two antennas," *IEEE Antennas Wireless Propag. Lett.*, vol. 4, pp. 97–99, 2005.
[56] S. Blanch, J. Romeu, and I. Corbella, "Exact representation of antenna system diversity performance from input parameter description," *Electron. Lett.*, vol. 39, no. 9, pp. 705–707, May 2003.
[57] D. Sarkar, and K. V. Srivastava, "Application of cross-correlation greens function along with FDTD for fast computation of envelope correlation coefficient over wideband for MIMO antennas," *IEEE Trans. Antennas Propag.*, vol. 65, no. 2, pp. 730–740, Feb. 2017.
[58] K. Zhao, S. Zhang, K. Ishimiya, Z. Ying, and S. He, "Body-insensitive multimode MIMO terminal antenna of double-ring structure," *IEEE Trans. Antennas Propag.*, vol. 63, no. 5, pp. 1925–1936, May 2015.
[59] S. Zhang, K. Zhao, Z. Ying, and S. He, "Investigation of diagonal antenna-chassis mode in mobile terminal LTE MIMO antennas for bandwidth enhancement," *IEEE Antennas Propag. Mag.*, vol. 57, no. 2, pp. 217–228, Apr. 2015.
[60] S. Zhang, A. A. Glazunov, Z. Ying, and S. He, "Reduction of the envelope correlation coefficient with improved total efficiency for mobile LTE MIMO antenna arrays: Mutual scattering mode," *IEEE Trans. Antennas Propag.*, vol. 61, no. 6, pp. 3280–3291, Jun. 2013.
[61] M. Razmhosseini and R. G. Vaughan, "Accuracy of modeling for evaluation of an integrated diversity wireless system on a small PCB," in *Proc. IEEE Int. Symp. Antennas Propag. USNC/URSI Nat. Radio Sci. Meeting*, Jul. 2015, pp. 1230–1231.
[62] J. X. Yun and R. G. Vaughan, "Space efficiency of multiple element antennas," *IEEE Trans. Antennas Propag.*, vol. 60, no. 6, pp. 3066–3071, Jun. 2012.
[63] J. X. Yun and R. G. Vaughan, "Evaluating multi-element antennas using equivalent number of antenna elements," in *Proc. 7th Eur. Conf. Antennas Propag. (EuCAP)*, 2013, pp. 89–93.
[64] K. Zhao, S. Zhang, Z. Ying, T. Bolin, and S. He, "SAR study of different MIMO antenna designs for LTE application in smart mobile phones," in *Proc. IEEE Int. Symp. Antennas Propag.*, Jul. 2012, pp. 1–2.
[65] H. Li, X. Lin, B. K. Lau, and S. He, "Calculating signal correlation in lossy dipole arrays using scattering parameters and efficiencies," in *Proc. 7th Eur. Conf. Antennas Propag. (EuCAP)*, 2013, pp. 519–523.
[66] V. Papamichael, M. Karaboikis, C. Soras, and V. Makios, "Diversity and MIMO performance evaluation of compact multi element antennas with common phase center," in *Proc. 19th Int. Conf. Appl. Electromagn. Commun.*, 2007, pp. 1–4.
[67] A. Sibille, C. Oestges, and A. Zanella, *MIMO: From Theory to Implementation*. New York, NY, USA: Academic, 2010.
[68] C. Yuen and B. M. Hochwald, "Achieving near-capacity at low SNR on a multiple-antenna multiple-user channel," *IEEE Trans. Commun.*, vol. 57, no. 1, pp. 69–74, Jan. 2009.
[69] Z. Xia, N. Akil, C. W. Domier, N. C. Luhmann, and H. Park, "Wide bandwidth printed circuit imaging antenna arrays," in *Proc. Infr. Millim. Waves, Int. Conf. 12th Int. Conf. Terahertz Electron.*, 2004, pp. 561–562.
[70] C. Jiang and L. J. Cimini, "Antenna selection for energy-efficient MIMO transmission," *IEEE Wireless Commun. Lett.*, vol. 1, no. 6, pp. 577–580, Dec. 2012.
[71] O. Staub, J.-F. Zürcher, and A. Skrivervik, "Some considerations on the correct measurement of the gain and bandwidth of electrically small antennas," *Microw. Opt. Technol. Lett.*, vol. 17, no. 3, pp. 156–160, Feb. 1998.
[72] M. K. Khandelwal, B. K. Kanaujia, and S. Kumar, "Defected ground structure: Fundamentals, analysis, and applications in modern wireless trends," *Int. J. Antennas Propag.*, vol. 2017, Feb. 2017, Art. no. 2018527.
[73] A. K. Arya, M. V. Kartikeyan, and A. Patnaik, "Defected ground structure in the perspective of microstrip antennas: A review," *Frequenz*, vol. 64, pp. 79–84, Jun. 2010.
[74] P. R. Prajapati, "Application of defected ground structure to suppress out-of-band harmonics for WLAN microstrip antenna," *Int. J. Microw. Sci. Technol.*, vol. 2015, Nov. 2015, Art. no. 210608.
[75] K. Wei, J. Li, L. Wang, Z. Xing, and R. Xu, "S-shaped periodic defected ground structures to reduce microstrip antenna array mutual coupling," *Electron. Lett.*, vol. 52, no. 15, pp. 1288–1290, 2016.
[76] R. Anitha, V. P. Sarin, P. Mohanan, and K. Vasudevan, "Enhanced isolation with defected ground structure in MIMO antenna," *Electron. Lett.*, vol. 50, no. 24, pp. 1784–1786, 2014.
[77] J.-S. Row, S.-H. Yeh, and K.-L. Wong, "Compact dual-polarized microstrip antennas," *Microw. Opt. Technol. Lett.*, vol. 27, no. 4, pp. 284–287, 2000.
[78] C. R. Jetti and V. R. Nandanavanam, "Trident-shape strip loaded dual band-notched UWB MIMO antenna for portable device applications," *AEU-Int. J. Electron. Commun.*, vol. 83, pp. 11–21, Jan. 2018.
[79] F. G. Zhu, J. D. Xu, and Q. Xu, "Reduction of mutual coupling between closely-packed antenna elements using defected ground structure," *Electron. Lett.*, vol. 45, no. 12, pp. 601–602, Jun. 2009.
[80] Y. S. Chen and T. Y. Ku, "Development of a compact LTE dual-band antenna using fractional factorial design," *IEEE Antennas Wireless Propag. Lett.*, vol. 14, pp. 1097–1100, 2015.
[81] A. Petosa, *Dielectric Resonator Antenna Handbook*. Boston, MA, USA: Artech House, 2007.
[82] C. A. Balanis, *Antenna Theory: Analysis and Design*, 3rd ed. Hoboken, NJ, USA: Wiley, 2005.
[83] S. Keyrouz and D. Caratelli, "Dielectric resonator antennas: Basic concepts, design guidelines, and recent developments at millimeter-wave frequencies," *Int. J. Antennas Propag.*, vol. 2016, Sep. 2016, Art. no. 6075680.
[84] U. Ullah, M. F. Ain, and Z. A. Ahmad, "A review of wideband circularly polarized dielectric resonator antennas," *China Commun.*, vol. 14, no. 6, pp. 65–79, 2017.
[85] A. Petosa and A. Ittipiboon, "Dielectric resonator antennas: A historical review and the current state of the art," *IEEE Antennas Propag. Mag.*, vol. 52, no. 5, pp. 91–116, Oct. 2010.
[86] G. Das, A. Sharma, R. K. Gangwar, and M. S. Sharawi, "Compact back-to-back DRA-based four-port MIMO antenna system with bi-directional diversity," *Electron. Lett.*, vol. 54, no. 14, pp. 884–886, 2018.
[87] M. S. Sharawi, S. K. Podilchak, M. U. Khan, and Y. M. Antar, "Dual-frequency DRA-based MIMO antenna system for wireless access points," *IET Microw., Antennas Propag.*, vol. 11, no. 8, pp. 1174–1182, 2017.
[88] G. Das, A. Sharma, R. K. Gangwar, and M. S. Sharawi, "Triple-port, two-mode based two element cylindrical dielectric resonator antenna for MIMO applications," *Microw. Opt. Technol. Lett.*, vol. 60, no. 6, pp. 1566–1573, 2018.
[89] G. Das, A. Sharma, and R. K. Gangwar, "Dielectric resonator-based two-element MIMO antenna system with dual band characteristics," *IET Microw., Antennas Propag.*, vol. 12, no. 5, pp. 734–741, 2018.

[90] J. Bonache, I. Gil, J. García-García, and F. Martín, "Complementary split rings resonators (CSRRs): Towards the miniaturization of microwave device design," *J. Comput. Electron.*, vol. 5, nos. 2–3, pp. 193–197, Jul. 2006.

[91] R. Selvaraju, M. H. Jamaluddin, M. R. Kamarudin, J. Nasir, and M. H. Dahri, "Complementary split ring resonator for isolation enhancement in 5G communication antenna array," *Prog. Electromagn. Res.*, vol. 83, pp. 217–228, 2018.

[92] J. D. Baena *et al.*, "Equivalent-circuit models for split-ring resonators and complementary split-ring resonators coupled to planar transmission lines," *IEEE Trans. Microw. Theory Techn.*, vol. 53, no. 4, pp. 1451–1461, Apr. 2005.

[93] A. Ramachandran, S. V. Pushpakaran, M. Pezholil, and V. Kesavath, "A four-port MIMO antenna using concentric square-ring patches loaded with CSRR for high isolation," *IEEE Antennas Wireless Propag. Lett.*, vol. 15, pp. 1196–1199, 2016.

[94] M. S. Sharawi, M. U. Khan, A. B. Numan, and D. N. Aloi, "A CSRR loaded MIMO antenna system for ISM band operation," *IEEE Trans. Antennas Propag.*, vol. 61, no. 8, pp. 4265–4274, Aug. 2013.

[95] D.-G. Yang, D. O. Kim, and C.-Y. Kim, "Design of dual-band MIMO monopole antenna with high isolation using slotted CSRR for WLAN," *Microw. Opt. Technol. Lett.*, vol. 56, no. 10, pp. 2252–2257, 2014.

[96] A. Diallo, C. Luxey, P. Le Thuc, R. Staraj, and G. Kossiavas, "Study and reduction of the mutual coupling between two mobile phone PIFAs operating in the DCS1800 and UMTS bands," *IEEE Trans. Antennas Propag.*, vol. 54, no. 11, pp. 3063–3074, Nov. 2006.

[97] Y. Wang and Z. Du, "A wideband printed dual-antenna with three neutralization lines for mobile terminals," *IEEE Trans. Antennas Propag.*, vol. 62, no. 3, pp. 1495–1500, Mar. 2014.

[98] S.-W. Su, C.-T. Lee, and F.-S. Chang, "Printed MIMO-antenna system using neutralization-line technique for wireless USB-dongle applications," *IEEE Trans. Antennas Propag.*, vol. 60, no. 2, pp. 456–463, Feb. 2012.

[99] S. Wang and Z. Du, "Decoupled dual-antenna system using crossed neutralization lines for LTE/WWAN smartphone applications," *IEEE Antennas Wireless Propag. Lett.*, vol. 14, pp. 523–526, 2015.

[100] W. A. E. Ali and A. A. Ibrahim, "A compact double-sided MIMO antenna with an improved isolation for UWB applications," *AEU-Int. J. Electron. Commun.*, vol. 82, pp. 7–13, Dec. 2017.

[101] M. Kahrizi, T. K. Sarkar, and Z. A. Maricevic, "Analysis of a wide radiating slot in the ground plane of a microstrip line," *IEEE Trans. Microw. Theory Techn.*, vol. 41, no. 1, pp. 29–37, Jan. 1993.

[102] C.-X. Mao and Q.-X. Chu, "Compact coradiator UWB-MIMO antenna with dual polarization," *IEEE Trans. Antennas Propag.*, vol. 62, no. 9, pp. 4474–4480, Sep. 2014.

[103] S. T. Fan, Y. Z. Yin, B. Lee, W. Hu, and X. Yang, "Bandwidth enhancement of a printed slot antenna with a pair of parasitic patches," *IEEE Antennas Wireless Propag. Lett.*, vol. 11, pp. 1230–1233, 2012.

[104] J. S. Row and S. W. Wu, "Circularly-polarized wide slot antenna loaded with a parasitic patch," *IEEE Trans. Antennas Propag.*, vol. 56, no. 9, pp. 2826–2832, Sep. 2008.

[105] R. V. S. R. Krishna and R. Kumar, "A dual-polarized square-ring slot antenna for UWB, imaging, and radar applications," *IEEE Antennas Wireless Propag. Lett.*, vol. 15, pp. 195–198, 2016.

[106] R. V. S. R. Krishna and R. Kumar, "Microstrip fed square ring slot antenna for ultra-wideband dual polarisation with good isolation," *IET Microw., Antennas Propag.*, vol. 10, no. 7, pp. 791–796, 2016.

[107] T. K. Roshna, U. Deepak, V. R. Sajitha, K. Vasudevan, and P. Mohanan, "A compact UWB MIMO antenna with reflector to enhance isolation," *IEEE Trans. Antennas Propag.*, vol. 63, no. 4, pp. 1873–1877, Apr. 2015.

[108] S. Zhang, Z. Ying, J. Xiong, and S. He, "Ultrawideband MIMO/diversity antennas with a tree-like structure to enhance wideband isolation," *IEEE Antennas Wireless Propag. Lett.*, vol. 8, pp. 1279–1282, 2009.

[109] G. Srivastava and A. Mohan, "Compact MIMO Slot antenna for UWB applications," *IEEE Antennas Wireless Propag. Lett.*, vol. 15, pp. 1057–1060, 2016.

[110] M. S. Khan, A.-D. Capobianco, A. Iftikhar, R. M. Shubair, D. E. Anagnostou, and B. D. Braaten, "Ultra-compact dual-polarised UWB MIMO antenna with meandered feeding lines," *IET Microw., Antennas Propag.*, vol. 11, no. 7, pp. 997–1002, 2017.

[111] J.-Y. Zhang, F. Zhang, W.-P. Tian, and Y.-L. Luo, "ACS-fed UWB-MIMO antenna with shared radiator," *Electron. Lett.*, vol. 51, no. 17, pp. 1301–1302, 2015.

[112] D. E. Anagnostou, M. T. Chryssomallis, B. D. Braaten, J. L. Ebel, and N. Sepúlveda, "Reconfigurable UWB antenna with RF-MEMS for on-demand WLAN rejection," *IEEE Trans. Antennas Propag.*, vol. 62, no. 2, pp. 602–608, Feb. 2014.

[113] A. S. Kholapure and R. G. Karandikar, "Emerging techniques for printed reconfigurable antenna: A review," in *Proc. 2nd Int. Conf. Res. Comput. Intell. Commun. Netw. (ICRCICN)*, 2016, pp. 57–61.

[114] I. T. E. Elfergani, R. A. Abd-Alhameed, C. H. See, T. Sadeghpour, and S. M. R. Jones, "Reconfigurable antenna design approach for mobile applications and a technique for harmonics suppression," in *Proc. Loughborough Antennas Propag. Conf.*, 2011, pp. 1–4.

[115] S. Soltani, P. Lotfi, and R. D. Murch, "A port and frequency reconfigurable MIMO slot antenna for WLAN applications," *IEEE Trans. Antennas Propag.*, vol. 64, no. 4, pp. 1209–1217, Apr. 2016.

[116] R. Hussain, M. S. Sharawi, and A. Shamim, "An integrated four-element slot-based MIMO and a UWB sensing antenna system for CR platforms," *IEEE Trans. Antennas Propag.*, vol. 66, no. 2, pp. 978–983, Feb. 2018.

[117] R. Hussain, M. S. Sharawi, and A. Shamim, "4-element concentric pentagonal slot-line-based ultra-wide tuning frequency reconfigurable MIMO antenna system," *IEEE Trans. Antennas Propag.*, vol. 66, no. 8, pp. 4282–4287, Aug. 2018.

[118] J.-H. Lim, Z.-J. Jin, C.-W. Song, and T.-Y. Yun, "Simultaneous frequency and isolation reconfigurable MIMO PIFA using PIN diodes," *IEEE Trans. Antennas Propag.*, vol. 60, no. 12, pp. 5939–5946, Dec. 2012.

[119] A. N. Kulkarni and S. K. Sharma, "Frequency reconfigurable microstrip loop antenna covering LTE bands with MIMO implementation and wideband microstrip slot antenna all for portable wireless DTV media player," *IEEE Trans. Antennas Propag.*, vol. 61, no. 2, pp. 964–968, Feb. 2013.

[120] N. Jamaly, P.-S. Kildal, and J. Carlsson, "Compact formulas for diversity gain of two-port antennas," *IEEE Antennas Wireless Propag. Lett.*, vol. 9, pp. 970–973, 2010.

[121] Hitachi's Research & Development. *EBG Structure*. Accessed: Aug. 13, 2018. [Online]. Available: http://www.hitachi.com/rd/portal/glossary/e/ebg_structure.html

[122] Y. Rahmat-Samii, "Electromagnetic band gap (EBG) structures in antenna engineering: From fundamentals to recent advances," in *Proc. Asia–Pacific Microw. Conf.*, 2008, pp. 1–2.

[123] M. S. Alam, N. Misran, B. Yatim, and M. T. Islam, "Development of electromagnetic band gap structures in the perspective of microstrip antenna design," *Int. J. Antennas Propag.*, vol. 2013, Mar. 2013, Art. no. 507158.

[124] A. Suntives and R. Abhari, "Miniaturization and isolation improvement of a multiple-patch antenna system using electromagnetic bandgap structures," *Microw. Opt. Technol. Lett.*, vol. 55, no. 7, pp. 1609–1612, 2013.

[125] S. Ghosh, T.-N. Tran, and T. Le-Ngoc, "Dual-layer EBG-based miniaturized multi-element antenna for MIMO systems," *IEEE Trans. Antennas Propag.*, vol. 62, no. 8, pp. 3985–3997, Aug. 2014.

[126] B. Mohamadzade and M. Afsahi, "Mutual coupling reduction and gain enhancement in patch array antenna using a planar compact electromagnetic bandgap structure," *IET Microw., Antennas Propag.*, vol. 11, no. 12, pp. 1719–1725, 2017.

[127] J.-Y. Lee, S.-H. Kim, and J.-H. Jang, "Reduction of mutual coupling in planar multiple antenna by using 1-D EBG and SRR structures," *IEEE Trans. Antennas Propag.*, vol. 63, no. 9, pp. 4194–4198, Sep. 2015.

[128] F. Capolino, *Theory and Phenomena of Metamaterials*. Boca Raton, FL, USA: CRC Press, 2009.

[129] C. Caloz and T. Itoh, *Electromagnetic Metamaterials: Transmission Line Theory and Microwave Applications*. Hoboken, NJ, USA: Wiley, 2005.

[130] R. W. Ziolkowski, P. Jin, and C.-C. Lin, "Metamaterial-inspired engineering of antennas," *Proc. IEEE*, vol. 99, no. 10, pp. 1720–1731, Oct. 2011.

[131] G. Zhai, Z. N. Chen, and X. Qing, "Enhanced isolation of a closely spaced four-element MIMO antenna system using metamaterial mushroom," *IEEE Trans. Antennas Propag.*, vol. 63, no. 8, pp. 3362–3370, Aug. 2015.

[132] A. A. Ibrahim and M. A. Abdalla, "CRLH MIMO antenna with reversal configuration," *AEU-Int. J. Electron. Commun.*, vol. 70, no. 9, pp. 1134–1141, 2016.

[133] S. Xu, M. Zhang, H. Wen, and J. Wang, "Deep-subwavelength decoupling for MIMO antennas in mobile handsets with singular medium," *Sci. Rep.*, vol. 7, no. 1, 2017, Art. no. 12162.

[134] N. Kuwabara and Y. Hiroshima, "Development of coupling and decoupling networks below 150 kHz," in *Proc. Int. Symp. Electromagn. Compat.*, 1997, pp. 17–20.

[135] R. C. Marshall, "A new approach to coupling/decoupling networks for EMC testing," in *Proc. Int. Conf. Exhib. Electromagn. Compat. EMC York*, 1999, pp. 147–150.

[136] L. K. Yeung and Y. E. Wang, "Mode-based beamforming arrays for miniaturized platforms," *IEEE Trans. Microw. Theory Techn.*, vol. 57, no. 1, pp. 45–52, Jan. 2009.
[137] J. Andersen and H. Rasmussen, "Decoupling and descattering networks for antennas," *IEEE Trans. Antennas Propag.*, vol. AP-24, no. 6, pp. 841–846, Nov. 1976.
[138] L. Zhao, L. K. Yeung, and K.-L. Wu, "A novel second-order decoupling network for two-element compact antenna arrays," in *Proc. Asia–Pacific Microw. Conf.*, 2012, pp. 1172–1174.
[139] M. S. Khan, A.-D. Capobianco, A. I. Najam, I. Shoaib, E. Autizi, and M. F. Shafique, "Compact ultra-wideband diversity antenna with a floating parasitic digitated decoupling structure," *IET Microw., Antennas Propag.*, vol. 8, no. 10, pp. 747–753, Jul. 2014.
[140] K.-L. Wong, C.-Y. Tsai, and J.-Y. Lu, "Two asymmetrically mirrored gap-coupled loop antennas as a compact building block for eight-antenna MIMO array in the future smartphone," *IEEE Trans. Antennas Propag.*, vol. 65, no. 4, pp. 1765–1778, Apr. 2017.
[141] D. Wu, S. W. Cheung, Q. L. Li, and T. I. Yuk, "Decoupling using diamond-shaped patterned ground resonator for small MIMO antennas," *IET Microw., Antennas Propag.*, vol. 11, no. 2, pp. 177–183, 2017.
[142] L. Zhao and K.-L. Wu, "A decoupling technique for four-element symmetric arrays with reactively loaded dummy elements," *IEEE Trans. Antennas Propag.*, vol. 62, no. 8, pp. 4416–4421, Aug. 2014.
[143] L. Zhao and K.-L. Wu, "A dual-band coupled resonator decoupling network for two coupled antennas," *IEEE Trans. Antennas Propag.*, vol. 63, no. 7, pp. 2843–2850, Jul. 2015.
[144] C. F. Ding, X. Y. Zhang, C. D. Xue, and C. Y. D. Sim, "Novel pattern-diversity-based decoupling method and its application to multi-element MIMO antenna," *IEEE Trans. Antennas Propag.*, vol. 66, no. 10, pp. 4976–4985, Oct. 2018.
[145] H.-P. Li, G.-M. Wang, T. Cai, J.-G. Liang, and X.-J. Gao, "Phase- and amplitude-control metasurfaces for antenna main-lobe and side-lobe manipulations," *IEEE Trans. Antennas Propag.*, vol. 66, no. 10, pp. 5121–5129, Oct. 2018.
[146] H.-P. Li, G.-M. Wang, X.-J. Gao, J.-G. Liang, and H.-S. Hou, "A novel metasurface for dual-mode and dual-band flat high-gain antenna application," *IEEE Trans. Antennas Propag.*, vol. 66, no. 7, pp. 3706–3711, Jul. 2018.

IRAM NADEEM received the B.S. degree in electrical engineering and the M.S. degree in telecommunication engineering (major in optical fiber communication) from the University of Engineering and Technology Taxila, Pakistan, in 2010 and 2014, respectively, and the M.Eng. degree in information and communication engineering from Chosun University, South Korea, in 2018. She had worked as a lecturer and a lab engineer in different engineering institutes of Pakistan. She is currently a Research Associate with the Department of Information and Communication Engineering, Chosun University. Her research interests include optical fiber communication, microwave and satellite communication, ultra-wide band, multiple-input-multiple-output antenna design, and WPT.

DONG-YOU CHOI received the B.S., M.S., and Ph.D. degrees from the Department of Electronics Engineering, Chosun University, Gwangju, South Korea, in 1999, 2001, and 2004, respectively. Since 2006, he has been a Professor and a Researcher with the Information and Communication Engineering Department, Chosun University. His research interests include rain attenuation, antenna design, wave propagation, and microwave and satellite communication. He is a member of the IEICE, JCN, KEES, IEEK, KICS, and ASK.